Study of Human Orexin-1 and -2 G-Protein-Coupled Receptors with Novel and Published Antagonists by Modeling, Molecular Dynamics Simulations, and Site-Directed Mutagenesis

Alexander Heifetz,*,[†] G. Benjamin Morris,[§] Philip C. Biggin,[§] Oliver Barker,[†] Tara Fryatt,[†] Jonathan Bentley,[†] David Hallett,[†] Dominique Manikowski,[‡] Sandeep Pal,[†] Rita Reifegerste,[‡] Mark Slack,[‡] and Richard Law[†]

[†]Evotec (U.K.) Ltd., 114 Milton Park, Abingdon, Oxfordshire OX14 4SA, United Kingdom
[‡]Evotec AG, Manfred Eigen Campus, Essener Bogen 7, 22419 Hamburg, Germany
[§]Department of Biochemistry, University of Oxford, South Parks Road, Oxford OX1 3QU, United Kingdom

ABSTRACT: The class A G-protein-coupled receptors (GPCRs) Orexin-1 (OX1) and Orexin-2 (OX2) are located predominantly in the brain and are linked to a range of different physiological functions, including the control of feeding, energy metabolism, modulation of neuro-endocrine function, and regulation of the sleep–wake cycle. Site-directed mutagenesis (SDM) and domain exchange (chimera) studies have provided important insight into key features of the OX1 and OX2 binding sites. However, the precise determinants of antagonist binding and selectivity are still not fully known. In this work, we used homology modeling of OX receptors to direct further SDM studies. These SDM studies were followed by molecular dynamics (MD) simulations to rationalize the full scope of the SDM data and to explain the role of each mutated residue in the binding and selectivity of a set of OX antagonists: Almorexant (dual OX1 and OX2 antagonist), SB-674042 (OX1 selective antagonist), EMPA (OX2 selective antagonist), and others. Our primary interest was focused on transmembrane helix 3 (TM3), which is identified as being of great importance for the selectivity of OX antagonists. These studies revealed conformational differences between the TM3 helices of OX1 and OX2, resulting from differences in amino acid sequences of the OX receptors that affect key interhelical interactions formed between TM3 and neighboring TM domains. The MD simulation protocol used here, which was followed by flexible docking studies, went beyond the use of static models and allowed for a more detailed exploration of the OX structures. In this work, we have demonstrated how even small differences in the amino acid sequences of GPCRs can lead to significant differences in structure, antagonist binding affinity, and selectivity of these receptors. The MD simulations allowed refinement of the OX receptor models to a degree that was not possible with static homology modeling alone and provided a deeper rationalization of the SDM data obtained. To validate these findings and to demonstrate that they can be usefully applied to the design of novel, very selective OX antagonists, we show here two examples of antagonists designed in house: EP-109-0092 (OX1 selective) and EP-009-0513 (OX2 selective).
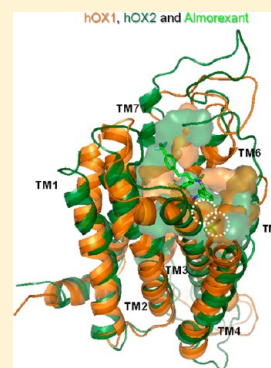
The class A G-protein-coupled receptors Orexin-1 (OX1) and Orexin-2 (OX2) are located predominantly in the hypothalamus and locus coeruleus[1,2] but are also found elsewhere in the CNS.[3−5] The Orexin receptors are highly conserved across mammalian species.[6−13] The human OX1 and OX2 receptors display 64% overall sequence identity, with 84% identity in the transmembrane regions.[14] The sequence alignment of hOX1 versus hOX2 is shown in Figure 1A. The OX receptors are linked to a range of different physiological functions, including the control of feeding, energy metabolism, modulation of neuroendocrine function,[15,16] and regulation of the sleep–wake cycle.[17−19] They are also associated with dopaminergic neurons of the ventral tegmental area (VTA)[20] that are critical elements of the reward system.[21] This dopaminergic pathway[22,23] is activated by drugs of abuse, and a number of studies indicate a critical role for OX1 receptor signaling in neuronal pathways,[24] leading to addiction and hence to the potential use of OX1 receptor antagonists in the

treatment of drug dependence.[25,26] Although the hypothalamic OX system is known to regulate appetitive behaviors[27,28] and promote wakefulness and arousal,[29] this system may also be important in adaptive and pathological anxiety–stress responses.[30,31] For instance, increasing Orexin concentrations in the brain of rats increases anxiety-like behavior.[31] Furthermore, in a recent study, Johnson et al.[32] determined that the Orexin system was hyperactive in an established rat model of panic vulnerability, and pharmacologically blocking the OX1 receptor or genetically silencing the Orexin system provoked panic- and anxiety-associated responses.
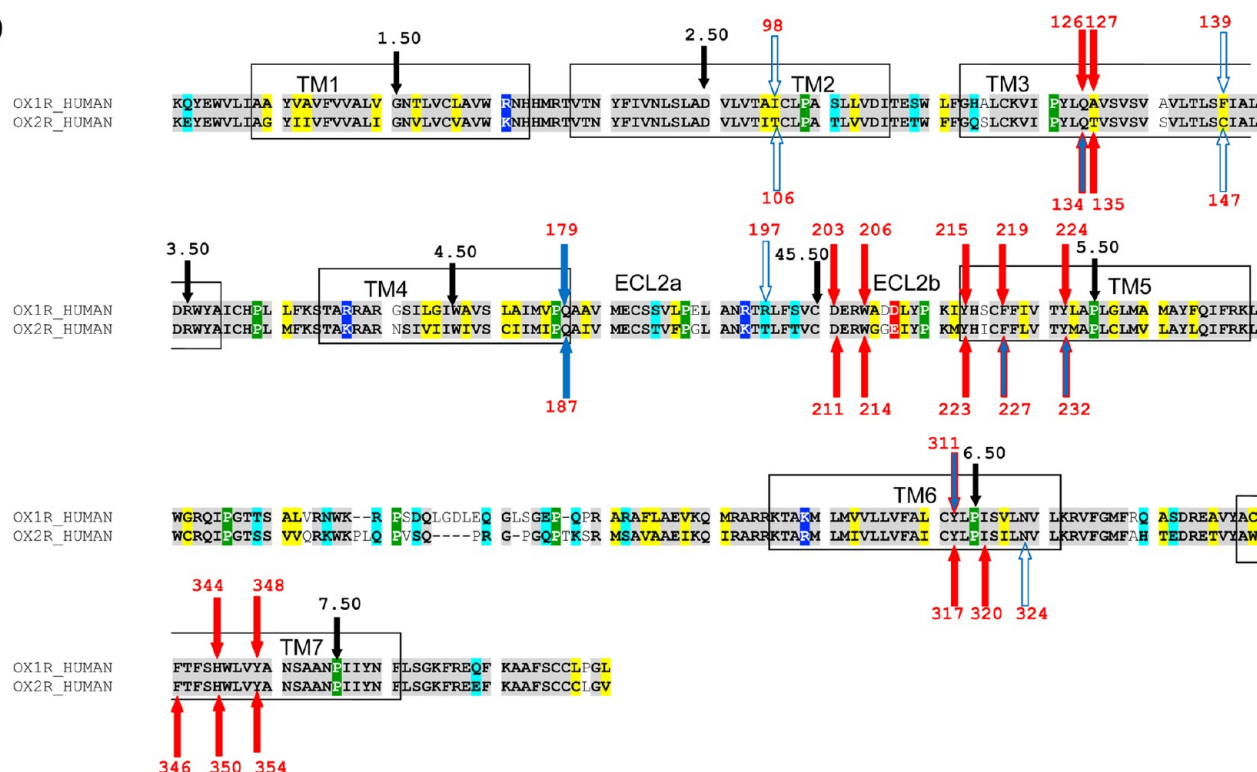
The hypothalamic neuropeptides Orexin-A/Hypocretin-1 (33 amino acids)[33] and Orexin-B/Hypocretin-2 (28 amino acids)[34] agonize their effect through OX1 and OX2 receptors

(A)

(B)

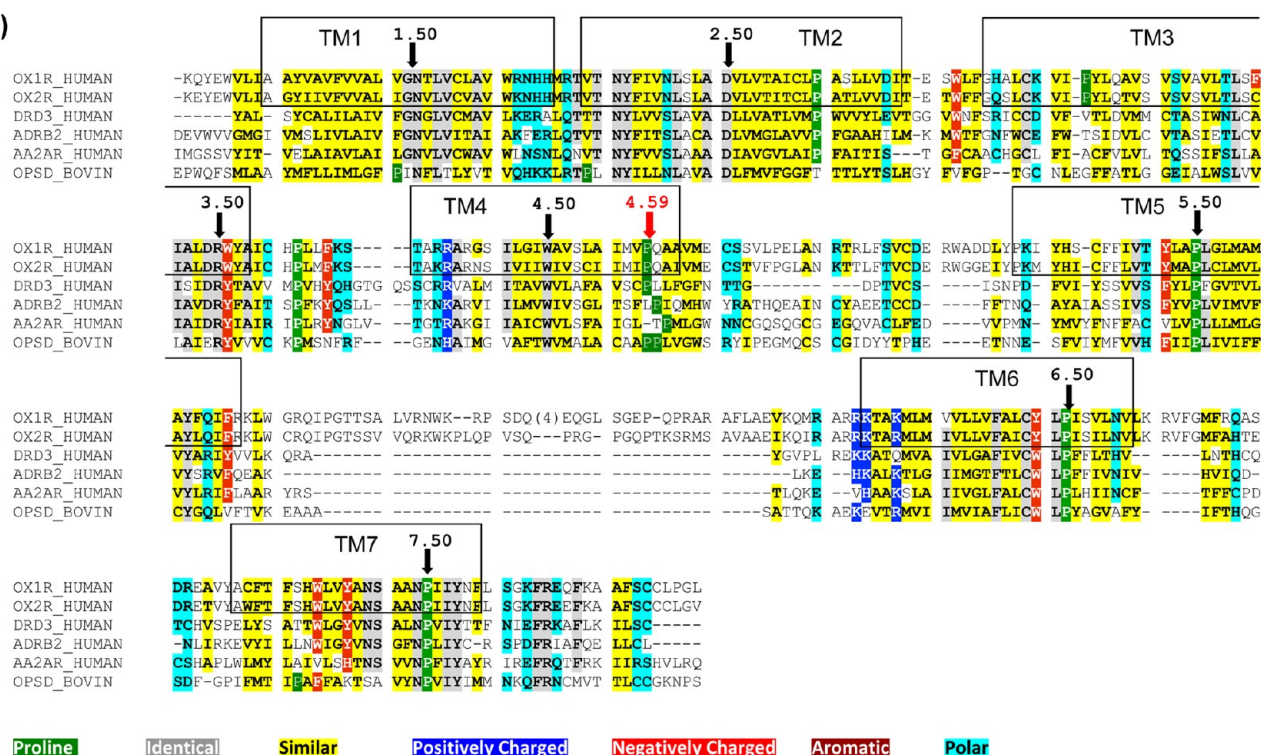**Figure 1.** (A) Amino acid sequence alignment of the TMD region of hOX1 (OX1R_HUMAN) with hOX2 (OX2R_HUMAN). The background color coding is as follows: gray for identical residues, yellow for chemically homologous residues, cyan for polar residues, blue for positive residues, red for negative residues, and green for prolines. The key residues that were involved in SDM are shown by colored arrows: red arrows for residues mutated by other researchers, blue arrows for mutations introduced by us, blue arrows with a red outline for mutations introduced by other researchers and by us, and white arrows with a blue outline for residues that the authors recommend for the future SDM study. The conserved residue in each TM that is assigned to 50 according to the Ballesteros−Weinstein numbering scheme is denoted with a black arrow. The red numbers are the amino acid numbers as they are appear in sequences of OX1 (O43613) and human OX2 (O43614), which were retrieved from the Swiss-Prot database. (B) Multiple-amino acid sequence alignment of the TMD region of hOX1 (OX1R_HUMAN) with hOX2 (OX2R_HUMAN) with crystal structures of GPCR receptors: human dopamine D3 receptor (DRD3_HUMAN), β2-adrenergic receptor (ADRB2_HUMAN), human A$_{2A}$ adenosine receptor (AA2AR_HUMAN), and bovine rhodopsin (OPSD_BOVIN). The background color coding is as follows: gray for identical

Figure 1. continued

residues, yellow for chemically homologous residues, cyan for polar residues, blue for positive residues, red for negative residues, orange for aromatic residues, and green for proline residues. The conserved residue in each TM that is assigned to 50 according to the Ballesteros—Weinstein numbering scheme is denoted with a black arrow. The key proline of TM4 is denoted with a red arrow.

that couple to $G_{q/11}$ and contribute to the activation of phospholipase C, leading to the elevation of intracellular Ca^{2+} concentrations.[35] It was recently determined that antagonism of the OX system is a novel mechanism for the treatment of insomnia.[36−40] Clinical investigation with Almorexant,[41,42] a dual OX1 and OX2 antagonist, indicated that this compound is highly efficacious in inducing and maintaining sleep.[43]

In light of this wide clinical evidence of the importance of OX receptors as potential drug targets,[43,44] the need for exploration of the key structural features and key residues of OX receptors involved in antagonist binding and selectivity cannot be overestimated. Such structural data are vital for driving the development of the next generation of new OX receptor antagonists.[45,46] Recently, several studies were conducted to address this issue, involving in silico guided site-directed mutagenesis[14] and domain exchange (chimera) studies[47,48] using EMPA,[49] JNJ-10397049[47] (OX2 selective antagonists), SB-674042[50] (OX1 selective antagonist), the dual antagonist Almorexant, and others as probes (see Table 1).

A total of 29 residues (11 in OX1 and 18 in OX2) located in TM2, -3, -5, -6, and -7 and extracellular loop (ECL) 2b regions were investigated via site-directed mutagenesis[14] (see Table 2). In the hOX1 receptor, among the 11 point mutations located in TM3, -5, -6, and -7 and ECL2b, mutations $Q126A^{3.32}$, $A127T^{3.33}$, $W206A^{45.54}$, $Y215A^{5.38}$, $F219A^{5.42}$, and $H344A^{7.39}$ eliminated the binding affinity and functional potency of both Almorexant and SB-674042 (the conventional superscript numbering refers to the Ballesteros—Weinstein numbering as outlined in Materials and Methods). The conserved residues $D203^{45.51}$, $Y224^{5.47}$, $Y311^{6.48}$, and $Y348^{7.43}$ of OX1 affected the two antagonists in different ways; the mutation of these residues had critical effects on Almorexant's binding and function but had no effect, or a weakened effect, on that of SB-674042.

In the hOX2 receptor, among the 18 point mutations[14] located in TM2, -3, -5, -6, and -7 and ECL2b (see Table 2), mutations $W214A^{45.54}$, $Y223A^{5.38}$, $F227A^{5.42}$, $Y317A^{6.48}$, and $H350A^{7.39}$ resulted in the complete loss of EMPA and Almorexant binding affinities. However, the mutation of $Y317^{6.48}$ to a phenylalanine had no significant effect on Almorexant binding but a small significant effect on EMPA binding affinity. The mutation $Y232A^{5.47}$ led to the complete loss of EMPA binding affinity and a significant decrease in EMPA potency yet had an only moderate effect on Almorexant binding affinity and potency. The mutations $T135A^{3.33}$, $I320A^{6.51}$, and $Y354A^{7.43}$ behaved differently with regard to the two antagonists in OX2, having a critical effect on the affinity and potency of EMPA, while the affinity and potency of Almorexant were not affected. Two mutations, $T111A^{2.61}$ and $D211A^{45.51}$, have a moderate effect on the binding of EMPA but no effect on that of Almorexant. The alanine mutation of OX2 residue $V138^{3.36}$ ($V130^{3.36}$ in OX1) affected the binding affinity and functional potency of EMPA (15- and 91-fold decreases, respectively) but had no effect on Almorexant binding in OX1 and OX2 or on binding of SB-674042 to OX1. It was concluded[14] that residues $T135^{3.33}$ and $V138^{3.36}$ are responsible for the selectivity of OX2 for EMPA.

The residue at position 3.33 is not conserved between the OX1 ($A127^{3.33}$) and OX2 ($T135^{3.33}$) receptors. Mutation of $A127^{3.33}$ to threonine dramatically affected the binding affinities and functions of SB-674042 and Almorexant at OX1; conversely, mutation of $T135^{3.33}$ of OX2 to alanine only reduced EMPA's binding affinity and potency. Hence, position 3.33 of OX receptors was identified[14,47] as a critical position that must be involved in subtype selectivity and also in differentiating two different antagonists for the same receptor, as observed for EMPA and Almorexant at OX2.
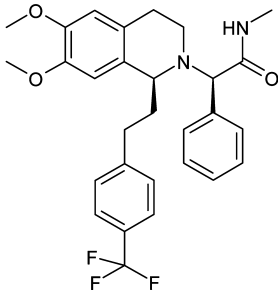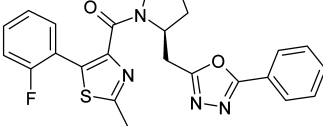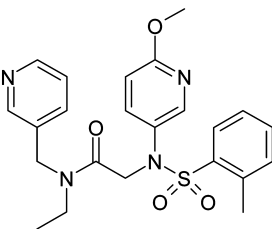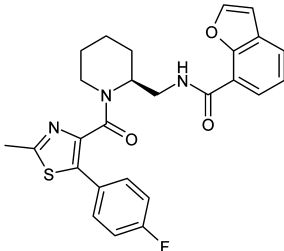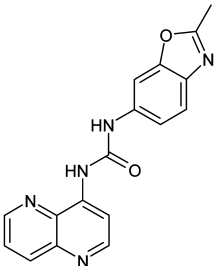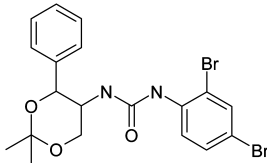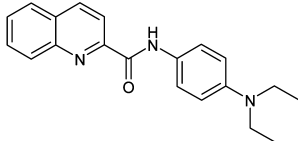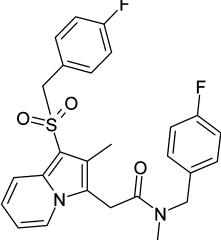
Alanine mutation of a conserved tyrosine residue located in TM7, at position 7.43 of both OX receptors, showed opposite effects in both receptors; while mutation of $Y348^{7.43}$ in OX1 eliminated Almorexant binding, the same mutation of $Y354^{7.43}$ had no effect on the binding affinity of Almorexant.

In a domain exchange (chimera) and SDM study performed by Tran et al.[47] with OX receptors, it was suggested that the Orexin antagonists occupy the same (orthosteric) binding site as the Orexin peptides. This study confirmed that TM2 and TM3 are important for selectivity between OX1 and OX2, particularly TM3 residues $Q134^{3.32}$ and $T135^{3.33}$. Antagonism of OX2 by JNJ-10397049 relies on the interactions with $Q134^{3.32}$ and $T135^{3.33}$. The $Q134A^{3.32}$ mutation causes a significant loss of functional activity for the Orexin peptides and selective OX2 antagonist JNJ-10397049, but little change for EMPA or SB-674042. Tran et al.[47] also observed that the $T231A^{5.46}$ mutation eliminates EMPA binding; however, as opposed to the work of Malherbe et al.,[14] the $V138A^{3.36}$ mutation in the OX2 receptor had no impact on EMPA activity. Furthermore, Tran et al.[47] observed that TM5, -6, and -7 also contribute key residues to the antagonist binding pocket. The mutations $I320A^{6.51}$, $S321A^{6.52}$, and $N324A^{6.55}$ impact EMPA and SB-674042 binding but have little effect on JNJ-10397049 activity. In TM7, $H350^{7.39}$ has a greater effect on OX2 antagonists than on SB-674042 while the $Y354A^{7.43}$ mutation impacts only EMPA activity.

These highly significant studies provided important insights into key structural features responsible for antagonist binding and selectivity. However, attempts to rationalize these contradictory experimental data through the use of static homology models of OX1 and OX2 receptors were less successful.[14]

Combining all of these disparate pieces of experimental data together into one full picture of knowledge and understanding is a vital stage in any structure-based drug discovery process. In this work, we attempted to address this issue by constructing homology models of the OX1 and OX2 receptors, using the high-resolution crystal structure of dopamine 3, D3, as a template, followed by molecular dynamics studies and flexible docking of the probe antagonists. In silico modeling can be a powerful tool for accurate prediction of GPCR structures as was recently demonstrated by Obiol-Perdo et al.[51] The availability of the recently determined crystal structure of D3 and the existence of SDM data, which were not previously available,[14] allowed the construction of high-resolution models of the OX receptors. These results reported here are comparable to those from other similar works[52−55] that showed that GPCR modeling[56−64] in the absence of a crystal structure

Table 1. OX1 and OX2 Antagonists[a]

Almorexant[41], Dual OX1/2 hOX1 IC$_{50}$* = 6.7 – 19 nM hOX2 IC$_{50}$* = 1.3 – 2.5 nM	**SB-674042** [50] OX1-sel hOX1 K$_b$ = 0.6 ± 0.1 nM	**EMPA OX2-sel** [49] hOX2 K$_b$ = 1.1 ± 0.1 nM
SB-649868 , Dual OX1/2 139, 140 hOX1 IC$_{50}$* = 1.5 – 2.1 nM hOX2 IC$_{50}$* = 89 – 128 nM	**SB-334867, Sel. OX1** [46] hOX1 IC$_{50}$* = 20.7 – 60 nM hOX2 IC$_{50}$* = N.D.B.	**JNJ-10397049** [47] hOX2 pK$_b$ = 7.0-7.8 nM
EP-109-0092, OX1-sel hOX1 K$_i$* = 36 nM hOX2 K$_i$* = N.D.B	**EP-009-0513, OX2-sel** hOX1 K$_i$* = 4363 nM hOX2 K$_i$* = 5.7 nM	

[a]Values denoted with asterisks were measured by us. N.D.B. means undetectable binding.

can be a valid replacement[65−72] for structural and functional exploration of the GPCR receptors,[60,70−79] and for the discovery,[54,73−76] virtual screening,[77−85] and optimization[56,86] of their ligands. Dynamic computational techniques such as

MD simulations followed by flexible docking have the potential to go beyond the use of static homology models[57,87−97] and allow a more detailed exploration of the GPCR structures. The MD simulations provided us with important insights into the

Table 2. Comparison of the Effects of Different Mutations on the hOX1 and hOX2 Binding Affinity of Almorexant, SB-674042, and EMPA[a]

position	hOX1	Almorexant	SB-674042	hOX2	Almorexant	EMPA
2.61				T111A[b]	=	↓
3.32	Q126A[b]	↓↓	↓	Q134A[b,c]	(↓),[b] (=)[c]	=
3.33	A127T[b]	↓↓	↓	T135A[b]	=	↓↓
3.36	V130A[b]	=	=	V138A[b]	=	↓
3.37				S139A[b]	=	=
4.60	Q179H[c]	↓				
4.60	Q179N[c]	=				
4.60	Q179A[c]	↑		Q187A[c]	↓	
45.51	D203A[b]	↓↓		D211A[b]	=	↓
45.54	W206A[b]	↓↓	↓↓	W214A[b]	↓↓	↓↓
5.38	Y215A[b]	↓↓	↓↓	Y223A[b,d]	↓↓	↓↓
5.42	F219A[b]	↓↓	↓↓	F227A[b,d]	↓↓	↓↓
5.43				F228A[b,d]	=	=
5.46				T231A[d]		↓↓
5.47	Y224A[b]	↓↓	=	Y232A[b]	↓	↓
				Y232F[c]	=	
6.48	Y311A[b]	↓↓	↓	Y317A[b]	↓↓	↓↓
6.48	Y311F[b,c]	=		Y317F[b]	↓	↓
6.51				I320A[b]	=	↓↓
7.35				F346A[b]	↑	=
7.39	H344A[b]	↓↓	↓	H350A[b]	↓↓	↓↓
7.42				V353A[b]	=	=
7.43	Y348A[b]	↓↓	↓	Y354A[b]	=	↓↓

[a]Legend: =, same potency as the wild type; ↓↓, no binding affinity; ↓, statistically significant decrease in binding affinity; ↑, increase in binding affinity. In bold are the mutations that have an opposite effect on antagonist binding in OX1 and OX2 receptors. [b]SDM data generated by Malherbe et al.[14] [c]SDM data generated by us and Evotec AG. [d]SDM data generated by Tran et al.[47]

interhelical interactions of OX receptors, the conformational changes of the 7TMD over time, and, in particular, the difference in the conformation of the TM3 helix between the OX1 and OX2 receptors.

We also extended the existing SDM data by performing our own *in silico* directed SDM study. Our particular interest was focused on position 4.60, located in the proximity of position 3.33 that was previously identified as being critical for antagonist binding and selectivity. Position 4.60 in TM4 is occupied by residues Q179$^{4.60}$ in OX1 and Q187$^{4.60}$ in OX2.

To validate these structural findings and to demonstrate that they can be usefully applied to the design of selective OX antagonists, we show here two examples of antagonists designed in house: EP-109-0092 (OX1 selective, Patent EP2161266) and EP-009-0513 (OX2 selective, Patent WO2011138265) (see Table 1).

MATERIALS AND METHODS

Residue Numbering. The position of each amino acid residue was identified both by its sequence number and by its generic number proposed by Ballesteros and Weinstein.[98] Briefly, in this numbering system, amino acid residues in the 7TMD are given two numbers; the first is the transmembrane (TM) helix number (1−7), while the second indicates the residue position relative to a highly conserved residue in class A GPCRs in that TM, which is arbitrarily assigned to be 50. The numbering of the loops is done in a similar manner; for example, extracellular loop 2 (ECL2) is labeled 45 to indicate its location between helices 4 and 5, and the conserved cysteine (thought to be part of a disulfide bond) is given the index number 45.50. The residues within the ECL2 loop are then numbered relative to this position.

Multiple-Sequence Alignment and Template Selection. This step is required for a selection of the optimal template, among the available GPCR crystal structures, for further homology modeling. The sequences of hOX1 and hOX2 were aligned with four published crystal structures of GPCR receptors [human dopamine D3 receptor (D3, PDB entry 3PBL),[99] β2-adrenergic receptor (β2AR, PDB entry 2RH1),[100] human A$_{2A}$ adenosine receptor (A$_{2A}$, PDB entry 3EML),[101] and bovine rhodopsin (PDB entry 1F88)[102]], using a multiple-sequence alignment tool implemented in MOE version 2010.10 (Chemical Computing Group). In this approach, originally introduced by Needleman,[103] alignments were computed by optimizing a function based on residue similarity scores obtained from applying an amino acid substitution matrix (blosum62)[104] to pairs of aligned residues and gap penalties. Penalties were imposed for introducing and extending gaps in one sequence with respect to another: the gap start penalty was set at 7, and the penalty for gap extension was set at 1. The conserved residues and conserved GPCR motifs were constrained to ensure their proper alignment. The amino acid sequences of human OX1 (O43613) and human OX2 (O43614) were retrieved from the SwissProt database. The position of each amino acid was identified by its sequence number and by the generic number proposed by Ballesteros and Weinstein.

Selection of the best template for GPCR modeling is usually very challenging.[70] Class A GPCRs share the same arrangement of seven helices,[105] and their levels of 7TMD sequence similarity are relatively high.[106−109] However, even small sequence differences can lead to significant differences in overall structure and particularly in the topology of the ligand

binding site.[110] This renders each GPCR unique to its exclusive biological function.

The most critical sequence difference in GPCRs is the difference in the positions of proline residues.[111−113] The prolines force kinks in TM secondary structure, and as a result, even the smallest difference in the positions of prolines in the sequence alignment of the modeled GPCR and the template can result in a significant decrease in the accuracy of the model.[112] We ranked the quality of crystal structures as potential templates for homology, based on the maximal number of correctly aligned prolines in the 7TMD. The crystal structure that had the highest number of aligned prolines was chosen as a template for further homology modeling.

Homology Modeling of OX Receptors. The modeling of hOX1 was performed using the homology modeling tool as implemented in MOE version 2010.10, based on the template selected in the previous stage. Because of insertions of the OX sequences with respect to the template, some residues, particularly in the loop regions, did not have assigned backbone geometries based on the template. These insertions were modeled from segments of high-resolution chains from the PDB that superposed well onto anchor residues on each side of the insertion area, after the method described by Fechteler.[114] Following the selection of appropriate loop templates, multiple model candidates for each loop were constructed and scored using a contact energy function. The coordinates of the top-ranked loop model were added to the global model. After all of the loops had been added, the side chains were modeled. Side chain data are assembled from an extensive rotamer library generated by systematic clustering of high-resolution PDB data. After all of the backbone segment and side chain conformations were chosen, and the model was minimized using the MMFF94x force field.[115] Homology modeling of hOX2 used the hOX1 model as the template. This was done to minimize the modeling noise between the OX receptors, to ease the comparison between the receptors, and to generate equal starting points for the further MD simulation study.

Molecular Dynamics Simulations. MD simulations were conducted with GROMACS version 4.5.4[116,117] using the OPLS-AA[118,119] force field and TIP3P water molecules[120] in a cubic box of 114 Å × 114 Å × 111 Å within periodic boundary conditions. Production simulations were performed in an *NPT* ensemble maintained at 310 K and a pressure of 1 bar. The integration time step was set to 2 fs, and a stochastic dynamics integrator[121] was used. Each receptor model was embedded in a 1-palmitoyl-2-oleoyl-*sn*-glycero-3-phosphocholine (POPC) bilayer using the *g_membed* feature of GROMACS.[122] Each system was energy minimized using a steepest descent algorithm, until convergence with a force tolerance of 0.239 kcal mol^{-1} Å^{-1}. Sodium and chloride ions were then added to the systems to a concentration of 150 nM. MD was then conducted with all heavy atoms restrained by a harmonic potential of 2.39 kcal mol^{-1} Å^{-2} for 200 ps, followed by a 50 ns production run with no restraints. During the position-restrained and production stages, the temperature and pressure were coupled using the Berendsen methods[123] and the temperatures were 323 and 310 K, respectively. Long-range electrostatics were calculated using the particle mesh Ewald (PME) method[124] with a 14 Å cutoff and 1 Å space grid. A cutoff of 9 Å was set for the Lennard-Jones potential, with a switch at 8 Å. The LINCS algorithm[125] was used to constrain bond lengths in both the lipid molecules and the protein. Initial velocities were assigned using a random seed to give a Maxwell

distribution corresponding to the temperature. We repeated the production stage three times for each OX receptor.

In this work to explore the behavior of different interactions over MD run, we used the softer definition of a hydrogen bond or salt bridge, which was defined as a case in which the distance between the hydrogen donor and hydrogen acceptor (between heavy atoms) is ≤3.5 Å.[126] The definition of an aromatic interaction is one in which the distance between centers of mass of aromatic atoms of two side chains is ≤5.5 Å.[127] The distances between residues were calculated using the *g_dist* function in GROMACS. These definitions were used to calculate the frequency of each interaction over the course of MD.

For crude evaluation of the difference in tilt between the cores of TM3^{OX1} and TM3^{OX2}, we measured an angle (θ) between the longest helix axes of TM3 in each receptor (see Figure 5C). We defined the TM3 core as the residues between Y$^{3.30}$ and L$^{3.48}$ in both receptors, i.e., those located between the flexible kink region induced by P$^{3.29}$ and the conserved helix−loop region of the DRY motif. The long helix axis corresponds to the eigenvector of the largest eigenvalue through a set of helix backbone atoms. The eigenvectors were calculated using the *rot3d_CovarianceEigenSystem* function in MOE version 2010.10.

Flexible Docking of Antagonists into OX Receptor Binding Sites. In this stage of our work, we aimed to optimize the conformations of the OX receptor binding site residues and to allow them to accommodate and interact with various antagonists. For these docking experiments, the MD refined homology models of OX1^{WT} and OX2^{WT} were harvested, after the root-mean-square deviation (rmsd) fluctuations of their Cα atoms reached stable plateaus (at 3 ns for OX1 and 12.9 ns for OX2). The structural data for the binding sites of OX receptors were obtained from SDM studies described by Malherbe et al.[14] Optimization of the OX antagonist binding pockets was performed by initial manual docking of Almorexant (dual OX1 and OX2 antagonist) into OX1 and OX2, SB-674042 (OX1 selective antagonist) into OX1, and EMPA (OX2 selective antagonist) into OX2, followed by minimization. To ensure that the TM helices do not "unwind" during the optimization, simple harmonic distance constraints were applied throughout the minimization to mimic the α-helical i, $i + 4$ carbonyl−amine hydrogen bonds. The OPLS-AA force field, which performs well[118,119] in the optimization of intermolecular interactions, was used during the minimization. Almorexant, SB-674042, and EMPA were redocked using the GOLD[128] docking package (Cambridge Crystallographic Data Centre). The default GOLD rotamer library was used to assign flexibility to chosen residues. Key residues selected to be flexible were D203$^{45.51}$, Y224$^{5.47}$, Y311$^{6.48}$, and Y348$^{7.43}$ for Almorexant docking and Q126A$^{3.32}$, W206$^{45.54}$, Y215$^{5.38}$, F219$^{5.42}$, and H344$^{7.39}$ for both Almorexant and SB-674042. Flexibility was allowed for key OX2 residues during the docking: in the case of EMPA docking, residues T135$^{3.33}$, I320$^{6.51}$, and Y354$^{7.43}$ were assigned to be flexible. In addition, residues W214$^{45.54}$, Y223$^{5.38}$, F227$^{5.42}$, Y232$^{5.47}$ Y317$^{6.48}$, and H350$^{7.39}$ were made flexible for docking of both EMPA and Almorexant into OX2.

To further optimize the interaction geometry between key residues and the antagonist and to optimize the conformation of the ECL2 loop, we used the LowModeMD[129] protocol. The LowModeMD protocol is a stochastic conformation generation protocol implemented in MOE. The starting point for this
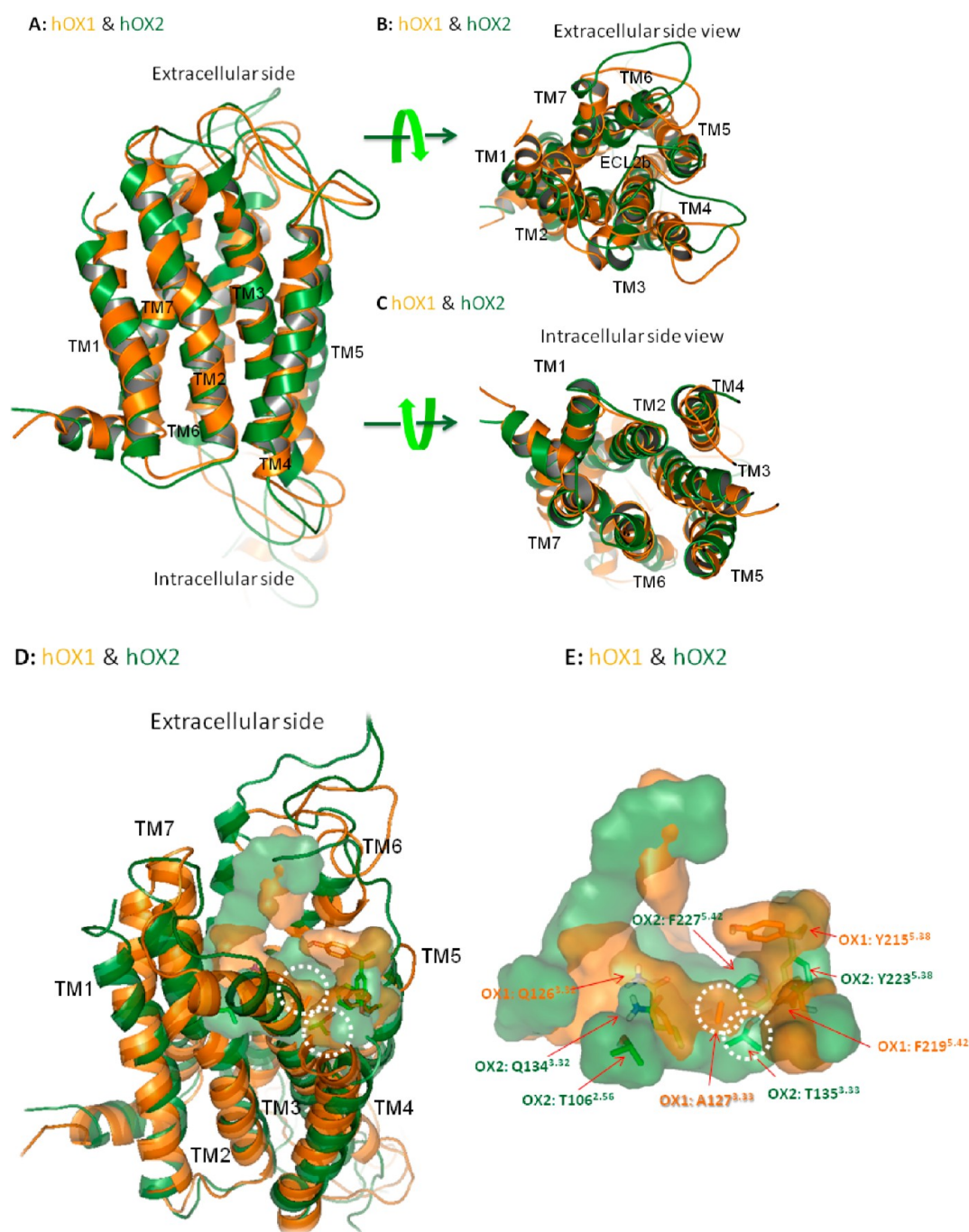
Figure 2. (A−C) Models of hOX1 (orange) and hOX2 (green) after MD for 50 ns. (D and E) Antagonist binding site of hOX1 (surface colored orange) and hOX2 (surface colored green). The key residues responsible for differences in site topology are shown as sticks. The key position 3.33 is outlined by white dashed circles.

refinement step was the top-ranked GOLD docking poses with optimized 7TMD key residues. During this process, the positions of the TM backbone atoms were restrained. The OPLS-AA force field was used for the conformational search, with the dielectric constant set to 3. A LowModeMD constant-temperature molecular dynamics simulation was performed at 300 K, using the Berendsen thermostat[123] and the velocity Verlet algorithm. The default value of the energy minimization gradient (0.001 kcal mol^{-1} Å^{-2}) was used. The LowModeMD and stochastic searches were terminated after 200 failed attempts to generate a new conformation, with a maximum of 10000 iterations.

Construction of Point-Mutated OX1 and OX2. Various mutations were introduced into the corresponding Orexin-1 and Orexin-2 cDNAs via a combination of mismatch and overlap PCR. Briefly, in the first step, each mutation was introduced into the gene sequence via the generation of two overlapping polymerase chain reaction (PCR) fragments with PfuUltra II Fusion HS DNA Polymerase (Strategene). Following gel extraction of the two products, a second round of PCR was performed via combining both fragments with 5′ and 3′ gene specific primers (containing BamHI and NotI restriction sites, respectively). The resulting gel-purified products were then cloned into expression vector pFB-Neo

for subsequent generation of stable cell lines. The sequence and integrity of each construct were confirmed via sequencing. Each verified cDNA was subsequently used to generate single, stable expressing clones in the CHO-K1 cell line.

Calcium Flux Assays. The functionality of each OX receptor mutant was assessed using a standard calcium flux assay and the corresponding stable expressing cell line. Each CHO-K1 Orexin mutant was seeded into tissue culture-treated, 384-well, black clear-bottom plates (CellBind Corning 7086), at a density of 7500 cells/well in culture medium, and maintained in an incubator (5% CO_2 at 37 °C) overnight. Cell medium was the removed, and the cells were incubated in 20 μL of assay buffer (4 μM Fluo-4AM in HBSS with 0.1% BSA) for 90 min at 37 °C. Following this incubation, the dye was removed and 45 μL of fresh buffer, without dye, was applied. For antagonists, 5 μL was then given, and after incubation at 37 °C for an additional 20 min, 20 μL of receptor specific agonists was applied and the calcium flux monitored using the Flex Station (Molecular Devices) over a period of 1 min. In all cases, the EC80 specific for the individual mutant, as determined in previous experiments, was applied.

■ RESULTS

Modeling of Human OX1 and OX2 Receptors. The homology model of the human OX1 receptor was modeled on the basis of a 2.8 Å high-resolution crystal structure of the dopamine D3 receptor (D3, PDB entry 3PBL). Of the possible templates available in the PDB at the time of writing, D3 shared the greatest number of aligned prolines (five in total) with both the hOX1 and hOX2 receptors, including the important proline at position 4.59.[100] The multiple-sequence alignment is shown in Figure 1B. Thus, D3 was preferred as a better template than the β2-adrenergic receptor used in other studies,[14] which has this proline at position 4.60. D3 has also a higher degree of sequence similarity with the hOX1 and hOX2 receptors than other GPCRs, 65.5% when comparing just the 7TMD region. The homology models of hOX2 and mutated A127T[3.33] hOX1 were constructed using the hOX1 model as a template (Figure 2). This was done to minimize the modeling noise between the OX receptors, to ease the comparison between them, and to generate equal starting points for the MD simulation studies. The three homology models obtained for the wild-type hOX1 (OX1[WT]), wild-type hOX2 (OX2[WT]), and mutated A127T[3.33] hOX1 (OX1[A127T]) receptors were employed as starting points for extensive MD simulations in an atomistic model of the membrane. These three models were validated by plotting their Cα atom rmsds as a function of time for the duration of the simulation (see the plot in Figure 3A). It was observed that after MD for 3 ns, the Cα atom fluctuations over time for all three models were within the same narrow range of 1.7–2.4 Å, which is comparable to the values typically obtained for MD simulations of GPCR crystal structures.[89] MD-refined homology models of OX1[WT] and OX2[WT] were harvested for the further docking experiments after the rmsd fluctuations of their Cα atoms reached stable plateaus; for OX1, this occurred after simulation for 3 ns, while for OX2, this required 12.9 ns.

TM3 Conformation in OX1[WT], OX1[A127T], and OX2[WT] Receptors. Previous SDM[14] and domain exchange studies[47] showed that TM3 plays a critical role in the selectivity of antagonists for OX1 versus OX2. The residue located at position 3.33 was noted to be of particular importance. This residue is not conserved between the OX1 (A127[3.33]) and OX2 (T135[3.33]) receptors. Mutation of A127[3.33] to threonine[14]
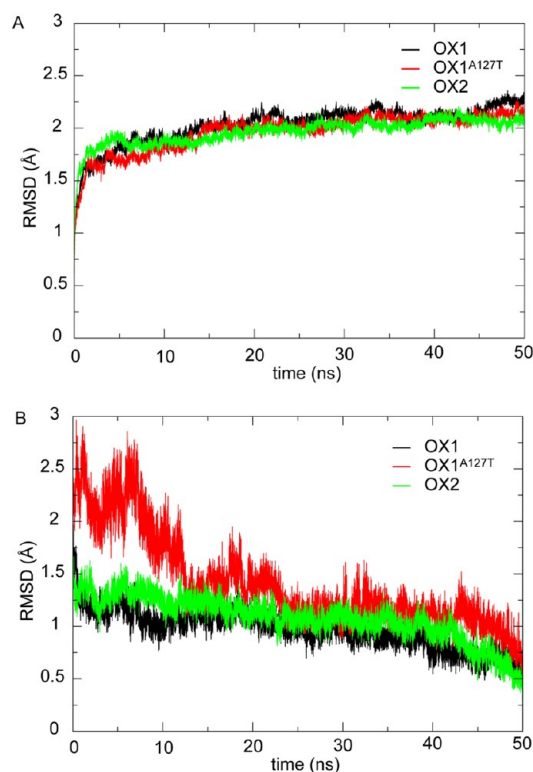

Figure 3. Plots of Cα atom rmsds vs time of the OX1[WT] (black), OX1[A127T] (red), and OX2[WT] (green) receptors. (A) rmsds of Cα atoms of the 7TMD compared to the initial frame. (B) rmsds of Cα atoms of the TM3 core defined between residues Y[3.30] and L[3.48] compared to the final frame at 50 ns. The TM helices excluding TM3 were used for alignment. All rmsds are averages of three simulation runs.

dramatically affected the binding affinities and functions of SB-674042 and Almorexant at OX1. Conversely, mutation of the residue at the same position in OX2 (T135[3.33]) to alanine eliminated the binding affinity and potency of EMPA but did not affect that of Almorexant.[14,47] Therefore, position 3.33 of OX receptors was identified as a critical position that must be involved in subtype selectivity as well as in differentiation of two different antagonists for the same receptor, as observed for EMPA and Almorexant with OX2.[14]

We explored the conformational change of TM3 in OX1[WT], OX1[A127T], and OX2[WT] over the course of the MD trajectory (see the plot in Figure 3B). We observed that, after MD for 10 ns, the TM3 Cα atom rmsds fluctuate within a narrow range between 1.0 and 1.5 Å for the OX1[WT], OX1[A127T], and OX2[WT] receptors. Such a small range of movement of Cα atoms indicates that the TM3 backbone conformation of OX1[WT], OX1[A127T], and OX2[WT] receptors is almost "frozen". The similarity between the Cα atom rmsds of OX1[WT] and OX1[A127T] indicates that the movement of the TM3 backbone is not significantly affected by the A127T[3.33] mutation.

To understand why the TM3 backbone conformation remained almost static during the MD simulation, we analyzed the type and frequencies of interhelical interactions formed between TM3 residues and the residues from its neighboring TMs. The results are summarized in Table 3 for each MD run. The starting point for this calculation was from the moment the Cα atom rmsds reached a stable plateau: 3 ns for OX1 and 12.9 ns for OX2. We observed that certain TM3 residues of OX1[WT] form specific interactions with residues of TM2 and TM7 that

Table 3. Interaction Frequencies in Percentages over the Three MD Runs

	hOX1			hOX2		
interaction pair	run 1	run 2	run 3	run 1	run 2	run 3
Hydrogen Bonds						
$N^{2.45}$–$W^{4.50}$	85%	98%	89%	99%	96%	100%
$N^{2.45}$–$T^{3.42}$	78%	65%	0%	94%	67%	97%
$T^{3.33}$ ($A^{3.33}$ in OX1)–$Y^{5.38}$				27%	74%	0%
$Q^{4.60}$–$Y^{5.38}$	33%	73%	82%	99%	95%	99%
$Q^{3.32}$–$Y^{7.43}$	0%	35%	28%	3%	0%	4%
$Q^{3.32}$–$T^{2.56}$ ($I^{2.56}$ in OX1)				0%	62%	0%
Aromatic Interaction						
$F^{2.42}$–$F^{3.45}$ ($C^{3.45}$ in OX2)	28%	66%	47%			
Salt Bridge						
$D^{45.51}$–$R^{45.45}$ ($T^{45.45}$ in OX2)	0%	99%	17%			

are not seen in OX2. These interactions are illustrated in panels A and B of Figure 4: an aromatic $\pi-\pi$ interaction between $F84^{2.42}$ and the nonconserved OX1 residue $F139^{3.45}$ (in OX2 it is $C147^{3.45}$), observed in three MD runs with frequencies of 28, 66, and 47%; and a hydrogen bond between $Q126^{3.32}$ and $Y348^{7.43}$ observed in two MD runs with frequencies of 35 and 28%.

The TM3 residues in $OX2^{WT}$ formed a set of specific interactions with the residues of TM2 and TM7 different from those seen in $OX1^{WT}$ (see Figure 4C,D). These were a hydrogen bond between $Q134^{3.32}$ and the nonconserved residue $T106^{2.56}$ (in OX1 this is $I98^{2.56}$), observed with 62% frequency in MD run 2, and a hydrogen bond between the nonconserved OX2 residue $T135^{3.33}$ (in OX1 it is $A127^{3.33}$) and

$Y223^{5.38}$ with frequencies of 27 and 74% in runs 1 and 2, respectively. The key differences in TM3 interhelical interactions between $OX1^{WT}$ and $OX2^{WT}$ are illustrated in panels A and B of Figure 5.

These different interhelical interactions force the core of $TM3^{OX1}$ and $TM3^{OX2}$ to adopt slightly different conformations (see Figure 5C). In OX2, there appeared to be a tilting of the $TM3^{OX2}$ core away from its original position in OX1, which could potentially be stabilized by the interaction between $Q134^{3.32}$ and, unique to OX2, residue $T106^{2.56}$ (see Figure 5B). However, analysis of the tilt angle did not reveal a direct correlation with the ability of this interaction to form. Nevertheless, the combined small motions in OX2 in this region create additional space among TM3, -4, and -5 in the antagonist binding site; as a result, the antagonist binding site in OX2 is wider than the binding site in OX1 (see Figure 2D,E). The subpocket among TM3, -4, and -5 also exists in $OX1^{WT}$, where $A127^{3.33}$ is a "gatekeeper" located at the entrance to this subpocket (see Figure 2C,D). Inside this subpocket, we find the key residues $Y215^{5.38}$, $F219^{5.42}$, and $Y224^{5.47}$, all of which are shown to be important for antagonist binding by SDM results. The mutation of $A127^{3.33}$ into the larger threonine residue limits the approach of the antagonist to this subpocket (see Figure 8B).

In spite of these differences, we observed that TM3 residues of OX1 and OX2 share a hydrogen bond network among $T136^{3.42}$, $N87^{2.45}$, and $W169^{4.50}$ that was clearly observed in all three runs of $OX1^{WT}$ MD simulations with high frequencies of $\geq 65\%$ (except for the $T136^{3.42}$–$Q87^{2.45}$ pair in MD run 3). This network is analogous to that observed in the MD simulations of $OX2^{WT}$ among $T144^{3.42}$, $N95^{2.45}$, and $W177^{4.50}$ in all three MD runs with high frequencies of $\geq 67\%$.

Predicted Mode of Binding of Almorexant with OX1 and OX2 Receptors. The proposed docking pose of
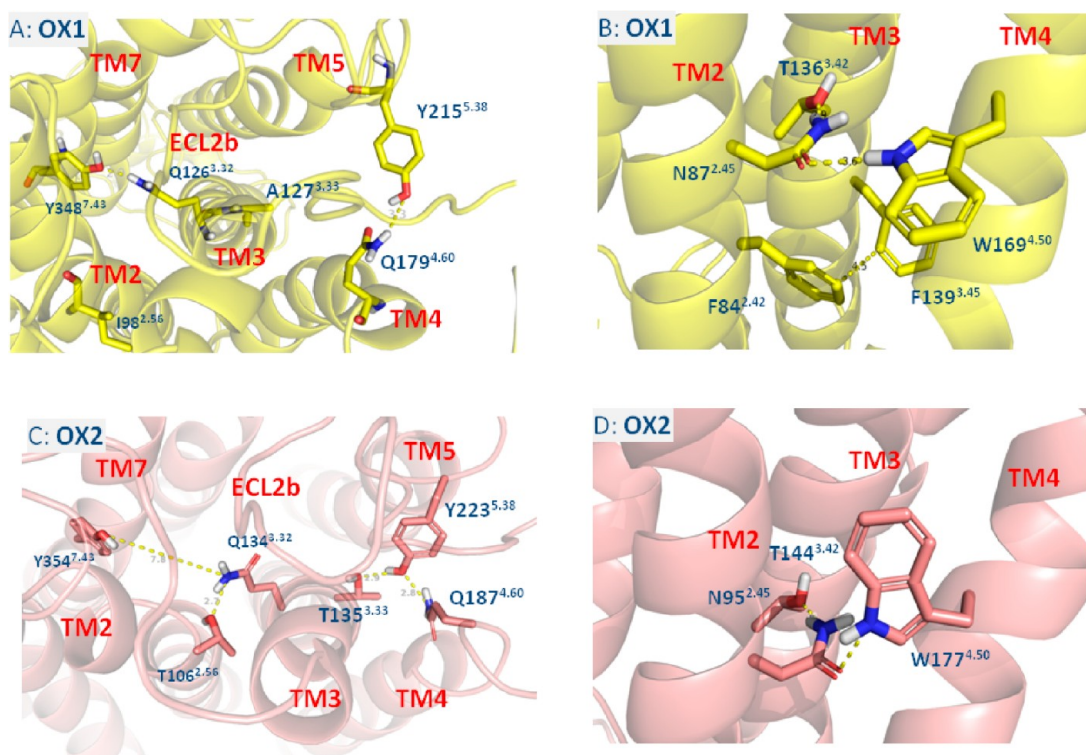

Figure 4. Interhelical interactions between residues of TM3 and residues of neighboring TMs in OX1 and OX2.
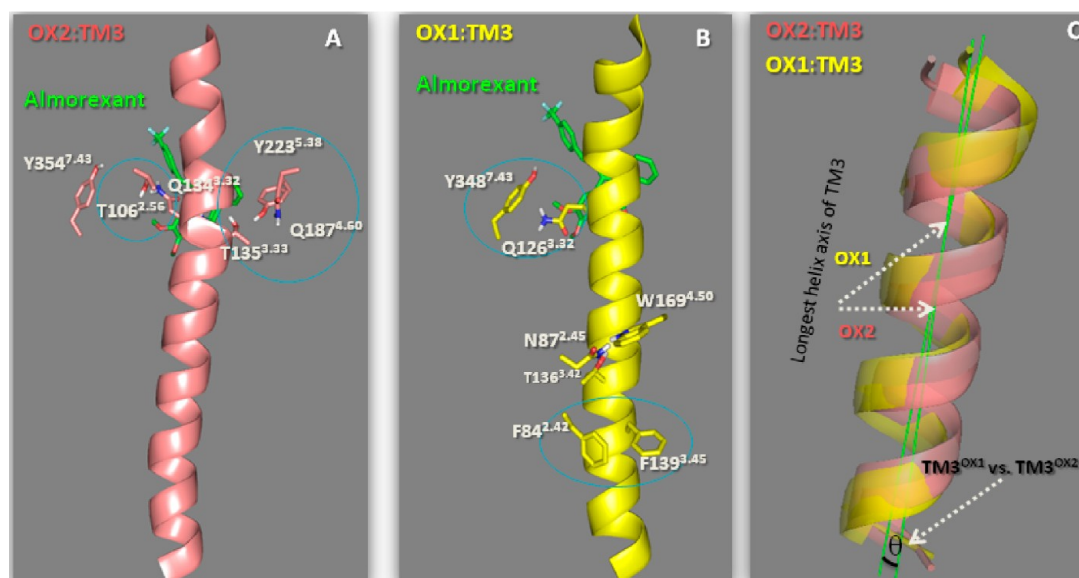
Figure 5. (A−C) Comparisons of the TM3 conformation in hOX1 vs hOX2 and the interactions that it forms with neighboring TMs. The backbones of TM3 in OX1 (yellow) and OX2 (orange) are represented as a cartoon. The residues that this study found to be important for stabilizing the unique conformation of each TM3 are shown. The blue circles emphasize the location of the specific key interactions. The predicted position of bound Almorexant is colored green. In panel C, the longest helix axes of TM3 are colored green and the θ angle between these two axes is colored black.
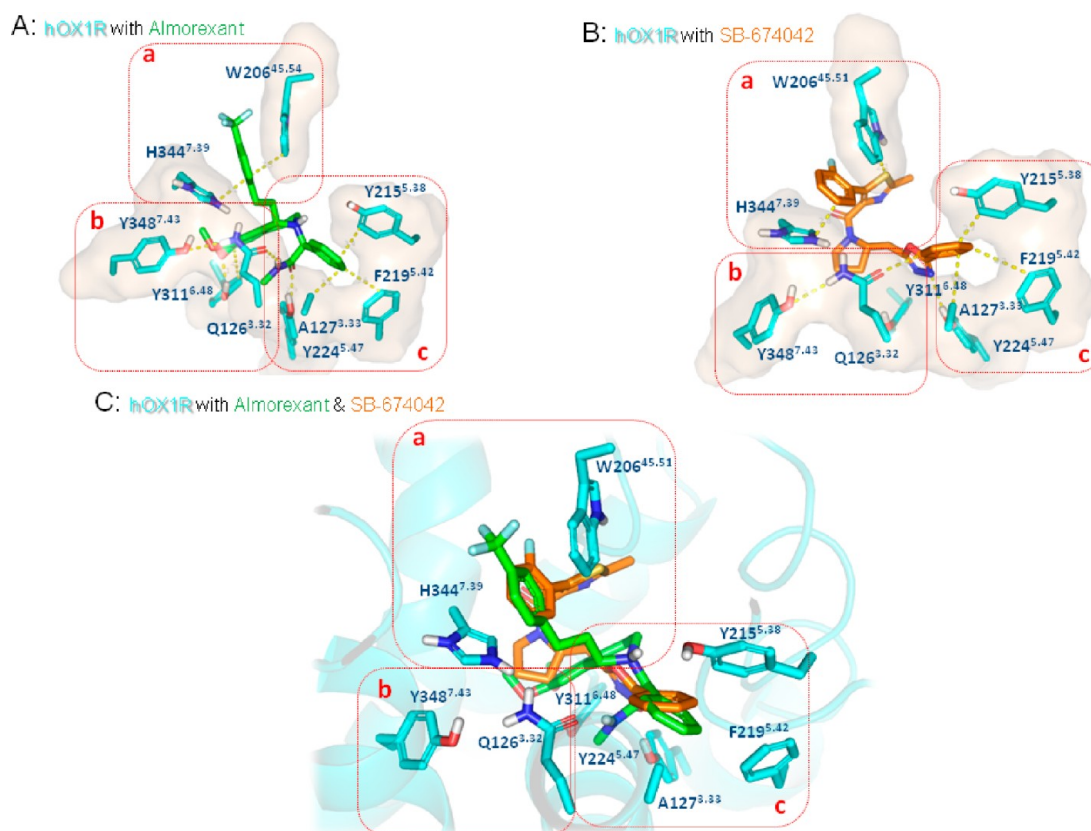

Figure 6. Predicted docking poses of Almorexant (A) and SB-674042 (B) in the OX1 binding site. The residues found to be important from SDM data are shown. Almorexant carbon atoms are colored green; the SB-674042 carbon is colored orange, and protein carbon atoms are colored cyan. Nitrogen atoms are colored blue, oxygens red, sulfurs yellow, and fluorines light green. The key interactions between protein and ligands are shown as yellow dashed lines. A Connolly surface was applied to key residues to show the surface topology of the antagonist binding site. (C) Predicted docking poses of both Almorexant (green) and SB-674042 (yellow) in the OX1 binding site. Colored orange are protein carbon atoms of residues that were important for Almorexant and SB-674042 according to SDM data. Nitrogens are colored blue, oxygens red, sulfurs yellow, and fluorines green.
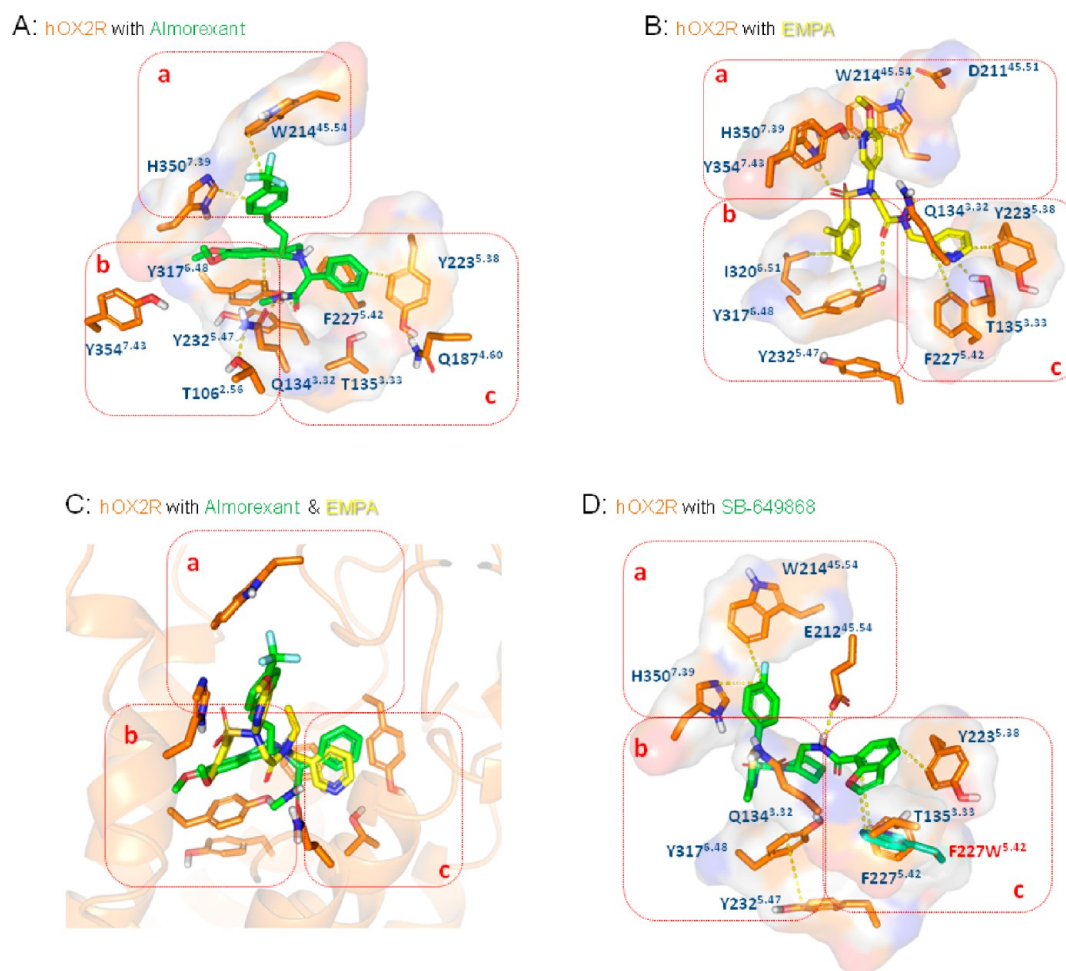
Figure 7. Predicted docking poses of Almorexant (A), EMPA (B), and SB-649868 (D) in the OX2 binding site. The residues found to be important according to SDM data are shown. Almorexant carbon atoms are colored green, the EMPA carbon atoms yellow, and protein carbon atoms orange. Nitrogen atoms are colored blue, oxygens red, sulfurs yellow, and fluorines light green. The key interactions between protein and ligands are shown as yellow dashed lines. A Connolly surface was applied to key residues to show the surface topology of the antagonist binding site. (C) Predicted docking poses of both Almorexant (green) and EMPA (yellow) in the OX2 binding site. Protein carbon atoms of residues that were important for Almorexant and EMPA binding according to SDM data are colored orange. Nitrogen atoms are colored blue, oxygens red, sulfurs yellow, and fluorines green.

Almorexant in the OX1 binding site is shown in Figure 6A. The Almorexant OX1 binding site is formed by TM3, -5, -6, and -7; it can be divided into three main regions, **a**, **b**, and **c**. In region **a**, the aromatic rings of residues $H344^{7.39}$ and $W206^{45.54}$ generate a $\pi-\pi$ interaction "sandwich" with the aromatic moiety of Almorexant. In region **b**, residue $Y311^{6.48}$ forms a mainly face-to-face $\pi-\pi$ interaction with Almorexant. This can be concluded from the fact that mutation of $Y311^{6.48}$ to alanine[14] resulted in a substantial decrease in the level of binding of Almorexant to OX1, while the mutation of this residue to phenylalanine (another aromatic residue) resulted in a negligible decrease in Almorexant affinity (see Table 2). An edge-to-face $\pi-\pi$ interaction of $Y311^{6.48}$ with Almorexant is not possible because of a steric clash with the ligand. $Q126^{3.32}$ generates a hydrogen bond with Almorexant and with $Y348^{7.43}$. $Y348^{7.43}$ does not form a direct interaction with Almorexant but still plays a key role by stabilizing $Q126^{3.32}$ in a conformation in which it interacts with Almorexant. The role of $D203^{45.51}$ is also not straightforward; on the basis of the model, it does not form a direct interaction with Almorexant but does generate a salt bridge with the unconserved residue $R197^{45.45}$ (in OX2 this is $T205^{45.45}$) that stabilizes the conformation of ECL2b. In region

c, the TM5 aromatic residues $Y215^{5.38}$ and $F219^{5.42}$ form face-to-face and edge-to-face $\pi-\pi$ interactions, respectively, with Almorexant. This bioactive conformation of $Y215^{5.38}$ is stabilized by a hydrogen bond with $Q179^{4.60}$ that is observed with high frequencies of $\geq 73\%$ in two MD runs (see Table 3). $Y224^{5.47}$ forms a hydrogen bond with Almorexant, while $A127^{3.33}$ makes a weak hydrophobic contact. Docking of Almorexant into mutated $OX1^{A127T}$ failed to generate a docking pose similar to that found for $OX1^{WT}$ (see Figure 8A). This is due to the fact that the $A127T^{3.33}$ mutation narrowed the entrance into the subpocket among helices TM3, -4, and -5 that is required for Almorexant binding in OX1 (see Figure 8B). This result supports the experimental evidence[14] that the $A127T^{3.33}$ mutation prevents binding of Almorexant to OX1.

The docking pose of Almorexant in the OX2 binding site is shown in Figure 7A. The Almorexant binding site in OX2 is formed by TM3, -5, -6, and -7; it can also be divided into three main regions, **a**, **b**, and **c**. In region **a**, the aromatic rings of residues $H350^{7.39}$ and $W214^{45.54}$ generate a face-to-face $\pi-\pi$ stack with the aromatic moiety of Almorexant. In region **b**, $Y317^{6.48}$ forms both a face-to-face $\pi-\pi$ interaction with the Almorexant core and a hydrogen bond with the carbonyl group.

Table 4. Effects of Point Mutations on the Potencies of OX Antagonists Relative (ratio) to the That of the Wild Type[a]

position	hOX1	Almorexant $IC_{50}^{MUT}/IC_{50}^{WT}$ dual	SB-649868 $IC_{50}^{MUT}/IC_{50}^{WT}$ dual	SB-334867 $IC_{50}^{MUT}/IC_{50}^{WT}$ OX1 sel.	hOX2	Almorexant $IC_{50}^{MUT}/IC_{50}^{WT}$ dual	SB-649868 $IC_{50}^{MUT}/IC_{50}^{WT}$ dual	SB-334867 $IC_{50}^{MUT}/IC_{50}^{WT}$ OX1 sel.
3.32	Q126A	NM	NM	NM	Q134A	0.31	0.21	NDB
4.60	Q179A	0.53	12.60	NM	Q187A	3.66	0.66	NDB
4.60	Q179H	8.94	24.00	0.98	Q187H	NM	NM	NM
4.60	Q179N	1.46	1.44	1.68	Q187N	NM	NM	NM
5.42	F219W	NM	NM	NM	F227W	NM	0.024	0.047[b]
5.47	Y224F	NM	NM	NM	Y232F	0.32	0.17	0.068[b]
6.48	Y311F	0.36	0.57	1.03	Y317F	NM	NM	NM

[a]Abbreviations: NDB, undetectable binding; NM, not measured. [b]In this case, the IC_{50}^{WT} value for calculation was taken to be 10000 nM (originally it was NDB).

This can be concluded from the fact that mutation of Y317[6.48] to alanine resulted in a substantial decrease in the level of binding of Almorexant to OX2,[14] while the mutation of this residue to phenylalanine (another aromatic residue) resulted in an only small decrease in Almorexant affinity[14] (see Table 2). Y232[5.47] does not form a direct interaction with Almorexant but stabilizes Y317[6.48] in a conformation in which it interacts with Almorexant. Q134[3.32] generates a weak hydrogen bond with Almorexant, and its conformation is stabilized by a hydrogen bond with T106[2.56]. Residue Y354[7.43] (in contrast to Y348[7.43] of OX1) is "unemployed" (see Figure 7A); it neither interacts directly with Almorexant nor stabilizes Q134[3.32] in a conformation that interacts with Almorexant (this job is fulfilled by the nonconserved residue T106[2.56]). In region **c**, TM5 aromatic residues Y223[5.38] and F227[5.42] both form face-to-face $\pi-\pi$ interactions with Almorexant. Interestingly, this bioactive conformation of Y223[5.38] is potentially stabilized by a hydrogen bond with Q187[4.60] (see Figure 7A), which is observed with high frequencies of ≥95% over all three MD runs (see Table 3). T135[3.33] generates a nonclassical hydrogen bond with the aromatic moiety of Almorexant.

Predicted Mode of Binding of SB-674042 with the OX1 Receptor. The docking pose of SB-674042 in the OX1 binding site is shown in Figure 6B. The SB-674042 OX1 binding site is formed by TM3, -5, -6, and -7. Its binding mode can be divided into three main regions, **a**, **b**, and **c**. In region **a**, residue H344[7.39] forms a face-to-face $\pi-\pi$ interaction with the benzyl moiety of SB-674042 and W206[45.54] generates a $\pi-\pi$ interaction with the thiazole moiety of SB-674042. In region **b**, Q126[3.32] generates a nonclassical hydrogen bond[130,131] with SB-674042 between its side chain carbonyl and the aromatic hydrogen of SB-674042. Residues Y311[6.48] and Y348[7.43] form a hydrophobic pocket that has good shape complementarity with the core of SB-674042. In region **c**, TM5 aromatic residues Y215[5.38] and F219[5.42] form face-to-face $\pi-\pi$ interactions with SB-674042. Y224[5.47] does not interact with SB-674042. A127[3.33] generates a weak hydrophobic contact with SB-674042.

Predicted Mode of Binding of EMPA with the OX2 Receptor. The docking pose of EMPA in the OX2 binding site is shown in Figure 7B. The EMPA binding site in OX2 is formed by TM3, -5, -6, and -7. Its binding mode can be divided into three main regions, **a**, **b**, and **c**. In region **a**, the residues H350[7.39] and W214[45.54] generate face-to-face and edge-to-face $\pi-\pi$ interactions, respectively, with the methoxypyridine moiety of EMPA. D211[45.51] does not generate a direct interaction with EMPA but forms a hydrogen bond with W214[45.54] that stabilizes the conformation in which that residue interacts with EMPA. H350[7.39] also forms a hydrogen bond with one of the oxygens from EMPA's SO_2 linker. The SO_2

linker may also form a hydrogen bond with N324[6.55]. An additional hydrogen bond is formed between Y354[7.43] and the nitrogen from the methoxypyridine moiety in EMPA. In region **b**, Y317[6.48] forms both an edge-to-face $\pi-\pi$ interaction with the benzyl moiety of EMPA and a hydrogen bond with the linker carbonyl. Y232[5.47] does not form a direct interaction with EMPA but stabilizes Y317[6.48] in a conformation where it can bind to EMPA. Residue I320[6.51] forms a CH$-\pi$ interaction with the benzyl moiety of EMPA, and Q134[3.32] does not form any direct interactions with EMPA. In region **c**, TM5 aromatic residues Y223[5.38] and F227[5.42] form $\pi-\pi$ interactions with EMPA. T135[3.33] forms a hydrogen bond with the nitrogen of the second pyridine moiety from EMPA.

Site-Directed Mutagenesis Results. We also extended the existing SDM data by performing our own *in silico* directed SDM study (see Table 4). Our particular interest was focused on residues at position 4.60, located in the proximity of position 3.33, which was previously identified[14] as being critical for antagonist binding and selectivity. Position 4.60 in TM4 is occupied by residues Q179[4.60] in OX1 and Q187[4.60] in OX2. A total of eight mutations (four in OX1 and four in OX2) located in TM2, -3, -4, -5, and -6 were explored (see Table 4). In the hOX1 receptor, of the four point mutations located in TM4, -5, and -6, the Q179H[4.60] mutation decreased the binding affinity of both Almorexant and SB-649868 but did not affect the binding of SB-334867.[139,140] The Q179A[4.60], Q179N[4.60], and Y311F[6.48] mutations showed almost no effect on the binding of any tested antagonist. In the hOX2 receptor, of the four point mutations located in TM3, -4, and -5, the Q187A[4.60] mutation significantly decreased the binding affinity of Almorexant and had almost no impact on the binding of SB-649868 or SB-334867. These data suggest that residue Q187[4.60] plays an important role in the binding of Almorexant to hOX2. The Q134A[3.32] mutation showed almost no effect on the binding of any tested antagonist. In contrast, the F227W[5.42] and Y232F[5.47] mutations significantly strengthen the binding of SB-649868 and SB-334867 to OX2 and Y232F[5.47] slightly improves the binding of Almorexant.

■ DISCUSSION

In this work, we demonstrate how the combination of homology modeling, MD simulations, and flexible docking is a highly efficient protocol for predicting the role of different residues and rationalizing the effect of their mutations on the binding of OX antagonists. As with other similar works,[52−55] this combination of experimental data with modeling techniques demonstrates that, in the absence of a crystal structure, GPCR modeling[56−64] can be a valid replace-
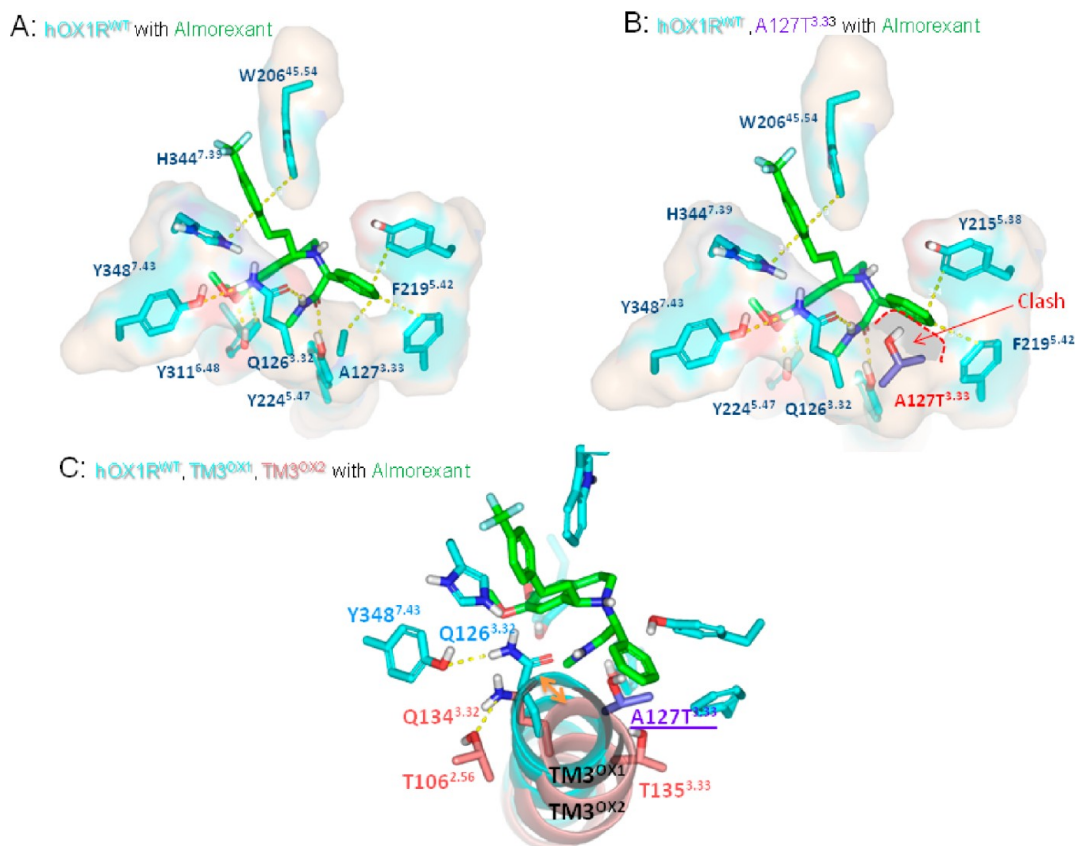
Figure 8. Docking poses of Almorexant in the binding site of OX1[WT], illustrating why binding of Almorexant to OX1[A127T] is not possible compared to binding to OX1[WT] and OX2[WT]. Only the residues found to be important from SDM data are shown. Almorexant carbon atoms are colored green, the protein carbon atoms cyan, and carbons of the A127T[3.33] mutant purple in panels B and C. Nitrogen atoms are colored blue, oxygens red, sulfurs yellow, and fluorines cyan. The key interactions are shown as yellow dashed lines. A Connolly surface was applied to key residues to show the surface topology of the antagonist binding site. (A) Almorexant in the binding site of OX1[WT]. (B) Almorexant in the binding site of OX1[WT], where the extra surface, generated by mutated T127, is colored gray and outlined by a red dashed line. (C) Difference in the TM3 backbone conformations in OX1[A127T] vs OX2[WT]. The backbones of TM3 in OX1[A127T] and OX2[WT] are represented by cyan and orange cartoons, respectively.

ment[65−68] for the structural exploration of GPCR receptors,[61,83,91,94,132−138] and for the discovery[54,73−76] and optimization[56,86] of their ligands. The MD simulations go beyond the use of static homology models and have allowed for a more detailed exploration of the OX structures and the differences between them. These simulations have provided us with important insights into interhelical interactions, the conformational changes in the 7TMD over time, and, in particular, the difference in TM3 conformation between the OX1 and OX2 receptors.

SDM data, summarized in Table 2, and domain exchange studies[47] revealed that TM3 plays a key role in OX subtype selectivity, particularly the residue located at position 3.33. We showed that different interhelical interactions force the backbone conformations of TM3[OX1] and TM3[OX2] to be different. The backbone conformation of TM3[OX2] is such that it allows additional space between TM3, -4, and -5 in the antagonist binding site of OX2, which in turn makes the antagonist binding site in OX2 wider than that in OX1 (see Figure 2C,D). A smaller subpocket among TM3, -4, and -5 also exists in OX1[WT] (see Figure 2E), with A127[3.33] located in a gatekeeper position. Inside this subpocket we find the key residues Y215[5.38], F219[5.42], and Y224[5.47] (see Figure 2E), which were identified by SDM studies[14] as being important for antagonist binding. The mutation of A127[3.33] to the larger residue threonine limits the approach of the antagonists to this

subpocket, resulting in the complete loss or a significant decrease in the level of binding of certain antagonists, such as Almorexant (see Figure 8C). This effect is probably unavoidable because of the limited mobility of the TM3 backbone as discussed earlier in Results. Some differences in conformation of other TMs between OX1 and OX2 are also observed (see Figure 2B,C).

The OX homology modeling, MD simulation, and flexible docking, paired with the SDM data, identified residues that have direct or indirect effects on antagonist binding. Direct effects resulted from mutation of the residues that form direct interactions with the ligand. The mutation of such residues usually weakened the binding of the antagonist to the receptor. Indirect effects resulted from mutation of residues that do not form direct interactions with the antagonist but that change the topology of the antagonist binding site and/or serve to stabilize other residues in a conformation where they form direct interactions with the ligand. The effect of such mutations on antagonist binding is somewhat harder to predict and can either strengthen or weaken antagonist binding.

OX1 residues Q126[3.32], W206[45.54], Y215[5.38], F219[5.42], Y224[5.47] (no effect on SB-674042 binding), Y311[6.48], and H344[7.39] form direct interactions with Almorexant (see Figure 6A) or SB-674042 (see Figure 6B). The other mutated residues, A127[3.33], D203[45.51], and Y348[7.43], have indirect effects on OX1 binding of Almorexant and/or SB-674042. While A127[3.33] forms a weak

hydrophobic contact with Almorexant and SB-674042, the effect of the mutation of this residue to threonine is primarily indirect. The direct loss of a weak hydrophobic contact is unlikely to lead to such a severe reduction in the level of antagonist binding, suggesting that an additional, more significant factor must be in play. As demonstrated by MD simulations, the $A127T^{3.33}$ mutation blocked the subpocket among TM3, -4, and -5, which is required for Almorexant and SB-674042 binding. The role of $D203^{45.51}$ is not clear but is probably indirect. On the basis of the MD-optimized model, it does not generate a direct interaction with Almorexant but does form a salt bridge with the unconserved residue $R197^{45.45}$ (in OX2 this is $T205^{45.45}$), which stabilizes the conformation of ECL2b. This salt bridge was observed with a high frequency (>99%) in run 2 of the OX1 MD simulation but was almost completely unobserved in runs 1 and 3 (see Table 3). Residue $Y348^{7.43}$ does not form a direct interaction with either Almorexant or SB-674042, but it still plays an indirect role by stabilizing $Q126^{3.32}$ in a conformation in which it can interact with the antagonists. The interaction between $Q126^{3.32}$ and $Y348^{7.43}$ was observed by MD with a frequency of >28% (see Table 3). The hypothesis that residues $Q126^{3.32}$ and $Y348^{7.43}$ are linked together in their effect on antagonist binding can be drawn from the SDM data,[14] as mutations of both have a severely negative effect on Almorexant binding but an only moderate effect on SB-674042 binding. The in-house point mutation $Q179H^{4.60}$ located in TM4 decreases the binding affinity of both Almorexant and SB-649868 but does not affect the binding of SB-334867. This is possibly due to the fact that this mutation of a flexible glutamine to a large and bulky histidine greatly reduces the amount of room available in the subpocket located among TM3, -4, and -5, which is required for Almorexant and SB-649868 binding, and also disturbs the bioactive conformation of $F219^{5.42}$. Mutation of $Q179^{4.60}$ to asparagine, a shorter residue with a similar chemical nature, did not have a significant effect on the binding of Almorexant, SB-649868, or SB-334867 to OX1. However, the mutation of $Q179^{4.60}$ to alanine, a shorter residue with a different chemical nature, resulted in a decrease in the level of binding of SB-649868 and had almost no effect on the binding of Almorexant. This was potentially due to an indirect effect. We observed that $Q179^{4.60}$ generates a stable hydrogen bond with $Y215^{5.38}$ with frequencies of 33, 73, and 82% in three MD runs (see Table 3); the $Q179A^{4.60}$ mutation resulted in the loss of this hydrogen bond and reduced the stability of the bioactive conformation of $Y215^{5.38}$ in which it forms a direct interaction with SB-649868.

OX2 residues $Q134^{3.32}$ [no effect on EMPA binding (see Table 2)], $Q135^{3.33}$, $W214^{45.54}$, $Y223^{5.38}$, $F227^{5.42}$, $Y317^{6.48}$, $I320^{6.51}$ [no effect on Almorexant binding (see Table 2)], $H350^{7.39}$, and $Y354^{7.43}$ [no effect on Almorexant binding (see Table 2)] form direct interactions with Almorexant (see Figure 7A) and/or EMPA (see Figure 7B). $Y317^{6.48}$ forms two interactions with Almorexant and EMPA, an aromatic $\pi-\pi$ interaction and a hydrogen bond. The $\pi-\pi$ interaction is the stronger of these two interactions, indicated by the severely negative effect of the $Y317A^{6.48}$ mutation on Almorexant and EMPA binding, compared to the moderate effect of the $Y317F^{6.48}$ mutation. The other mutated residues, $D211^{45.51}$, $Y232^{5.47}$, and $T231^{7.43}$, have an indirect effect on OX2 EMPA binding. $D211^{45.51}$ does not interact directly with EMPA but forms a hydrogen bond with $W214^{45.54}$, which stabilizes it in a conformation in which it can interact with EMPA. $Y232^{5.47}$ also does not form a direct interaction with EMPA but stabilizes

$Y317^{6.48}$ in the required conformation for EMPA binding. In the work of Tran et al.,[47] it was shown that $T231^{7.43}$ had a weakened effect on the OX2 binding of EMPA; we observed that the reason for this could be a nonclassical hydrogen bond formed between $T231^{7.43}$ and $F227^{5.42}$, which stabilizes $F227^{5.42}$ in a conformation in which it can interact with EMPA. In the hOX2 receptor, of the four in-house point mutations located in TM3, -4, and -5, the $Q187A^{4.60}$ mutation significantly decreased the binding affinity of Almorexant and had almost no effect on the binding of SB-649868 or SB-334867. We observed that the $Q187A^{4.60}$ mutation has an indirect effect on Almorexant binding. As was shown previously, the interaction between residues $Q187^{4.60}$ and $Y223^{5.38}$ (see Figure 4C) is very important for Almorexant binding. The $Q187A^{4.60}$ mutation resulted in the loss of the hydrogen bond with $Y223^{5.38}$ [a highly conserved hydrogen bond with a frequency of ≥95% in all three MD runs (see Table 3)] and destabilization of its bioactive conformation. The other in-house mutations, $F227W^{5.42}$ and $Y232F^{5.47}$, significantly strengthen the binding of SB-649868 and SB-334867 to OX2. The $F227W^{5.42}$ mutation potentially generates a tighter $\pi-\pi$ interaction in zone **c** with either the benzofuran moiety of SB-649868 (see Figure 7D) or the benzoxazole moiety of SB-334867. The reason for the improved binding effect of $Y232F^{5.47}$ is not clear, but it may be due to a steric or indirect electrostatic effect caused by the removal of the polar OH group from the $Y232^{5.47}$ residue.

These findings can help in the design of a new generation of selective and dual OX antagonists. The key difference between OX1 and OX2 antagonist binding is driven by the residues at positions 3.32 and 3.33 of TM3.[14] Position 3.33, in OX receptors, is occupied by different residues: $A127^{3.33}$ in OX1 and $T135^{3.33}$ in OX2. These residues can form different interactions with the antagonist; while $T135^{3.33}$ of OX2 can potentially form a hydrogen bond or OH−π interaction, $A127^{3.33}$ of OX1 can form only a weak hydrophobic interaction. Targeting an interaction with $T135^{3.33}$ of OX2 can assist in designing OX2 selective antagonists. Position 3.32 is occupied by a glutamine residue in both OX receptors: $Q126^{3.32}$ in OX1 and $Q134^{3.32}$ in OX2. However, because of the different TM3 tilted conformation of OX1 and OX2, the position of $Q126^{3.32}$ in OX1 is much more accessible for interactions with an antagonist than $Q134^{3.32}$ in OX2. Targeting an interaction with $Q126^{3.32}$ in OX1 is a possible strategy for the design of OX1 selective antagonists. An additional difference helpful in generating OX2 antagonist selectivity is the various roles played by $Y^{7.43}$; while in OX1 $Y348^{7.43}$ is involved in an interaction with $Q126^{3.32}$ and is thus less available to interact with the antagonist, $Y354^{7.43}$ of OX2 is completely free to interact with an antagonist. On the other hand, $Y224^{5.47}$ in OX1 is much more accessible to interact with antagonists than $Y232^{5.47}$ in OX2; this is also due to the difference in TM3 tilting. Targeting a hydrophobic interaction with residue $I320^{6.52}$ can also increase the OX2 selectivity of the antagonists. An additional difference between the OX receptors is the topology of their antagonist binding sites (see Figure 2C,D); this is primarily due to the different TM3 tilt conformation. OX1 has a narrow subpocket among TM3, -4, and -5 compared to the wide open space of OX2 in this region (see Figure 2D). This can also be exploited in the design of selective OX2 antagonists, for example, by attaching bulky groups that cannot be accommodated in the narrow pocket of OX1. Designing OX dual antagonists can be challenging and requires targeting of shared residues: $W^{45.54}$, $Y^{5.38}$, $F^{5.42}$, $Y^{6.48}$, and $H^{7.39}$.
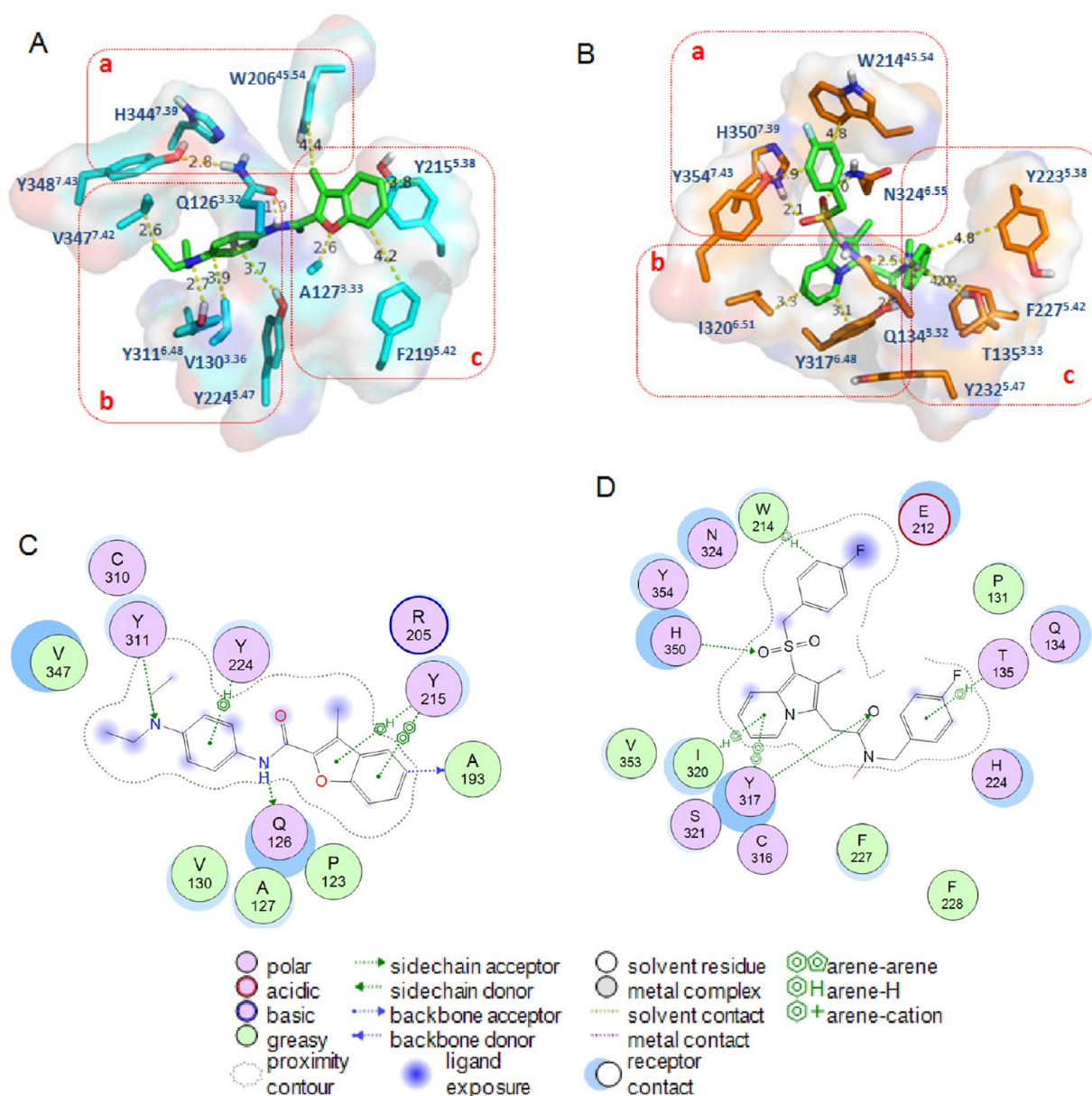
Figure 9. Predicted docking poses of EP-109-0092 (A) and EP-009-0513 (B) in the OX1 and OX2 binding sites, respectively. The residues found to be important according to docking and SAR are shown. Ligand carbon atoms are colored green, OX1 carbon atoms cyan, and OX1 carbon atoms orange. Nitrogen atoms are colored blue, oxygens red, sulfurs yellow, and fluorines light green. The key interactions between protein and ligands are shown as yellow dashed lines. A Connolly surface was applied to key residues to show the surface topology of the antagonist binding site. (C and D) Two-dimensional interaction maps of EP-109-0092 (C) and EP-009-0513 (D) in the OX1 and OX2 binding sites, respectively, generated with MOE.

To validate these structural findings and to demonstrate that they can be usefully applied to the design of novel and selective OX antagonists, we show here two examples of antagonists that we have designed in house: EP-109-0092 (OX1 selective, Patent EP2161266) and EP-009-0513 (OX2 selective, Patent WO2011138265) antagonists. These compounds are part of a wider SAR series not shown here, which will be reported in a future publication. The docking poses of EP-109-0092 and EP-009-0513 are shown in Figure 9.

The EP-109-0092−OX1 binding site (see Figure 9A) is positioned among TM3, -5, -6, and -7 and split into three key regions, **a**, **b**, and **c**. The two-dimensional (2D) interaction map of EP-109-0092 and OX1 is shown in Figure 9C. In this case, the residues of region **a** are much less involved in binding than they are with Almorexant and SB-6740042; the only residue

involved in binding is W206[45.54], which forms a hydrophobic contact with EP-109-0092. In region **b**, residues Q126[3.32] and Y311[6.48] form strong hydrogen bonds with EP-109-0092, Y224[5.38] forms an OH−π interaction with the benzyl group of the ligand, and V130[3.36] and V347[5.42] generate a hydrophobic sandwich with the same group. In region **c**, Y215[5.38] and F219[5.42] form an aromatic sandwich with the core of EP-109-0092.

The EP-009-0513−OX2 binding site (see Figure 9B) is positioned among TM3, -5, -6, and -7 and split into three key regions, **a**, **b**, and **c**. The 2D interaction map of EP-009-0513 and OX2 is shown in Figure 9D. In region **a**, the residues H350[7.39] and W214[45.54] form face-to-face and edge-to-face π−π interactions, respectively, with the aromatic moiety of EP-009-0513. H350[7.39] also forms a hydrogen bond with the SO$_2$ linker.

The SO_2 linker may also form a hydrogen bond with N324[6.55] in a manner similar to that of the SO_2 linker in EMPA. An additional nonclassical hydrogen bond is formed by Y354[7.43]. In region **b**, Y317[6.48] and I320[6.51] form edge-to-face $\pi-\pi$ and CH$-\pi$ interactions, respectively, with the benzyl moiety of EP-009-0513. In region **c**, T135[3.33] forms an OH$-\pi$ interaction with the aromatic moiety of EP-009-0513 and aromatic residues Y223[5.38] and F227[5.42] form $\pi-\pi$ interactions with EP-009-0513.

For future exploration, we suggest a new set of mutations (see Figure 1A), the T106I[2.56], T135A[3.33], and C147F[3.45] triple mutation; these mutations are predicted to convert the antagonist binding of OX2 into OX1-like, eliminating EMPA potency and improving that of SB-674042. Almorexant binding should not change. We also suggest an opposite experiment for OX1, with mutations I98T[2.56], A127T[3.33], and F139C[3.45]. Investigation of N324A[6.55] mutants is also of interest, because of the potential direct interaction between this residue and the SO_2 group in OX2 selective antagonists such as EP-009-0513 and EMPA. The hOX1 mutations F219W[5.42] and Y224F[6.55] are also very interesting as targets for future exploration, particularly their effect on the binding of Almorexant, SB-649868, SB-334867, and other dual or selective OX1 antagonists. The effect of the F227W[5.42] mutation on Almorexant binding is also an important piece of data for exploration. For hOX2, further exploration of how mutations Q187H[4.60] and Q187N[4.60] affect Almorexant binding is suggested, as well as their effect on the binding of OX2 antagonists that require residues T135[3.33] and Y223[5.38] and/or the subpocket among TM3, -4, and -5 for binding.

CONCLUSIONS

The MD simulation protocol used in our work, followed by flexible docking, has gone beyond the use of static homology models and allowed for a more detailed exploration of the OX structures. In this work, we have demonstrated how even minor differences in GPCR sequences can lead to significant differences in the tertiary structure of GPCRs, their ability to bind ligands, and their selectivity. The MD simulations allow refinement of the GPCR models to a degree that is not possible with static homology modeling alone. The structural insights gained from this process are critical for rationalizing the SDM data and for the design of a new generation of OX dual and selective antagonists.

AUTHOR INFORMATION

Corresponding Author
*Telephone: +44 (0)1235 83 89 25. Fax: +44 (0)1235 86 31 39. E-mail: Alexander.Heifetz@Evotec.com.

Notes
The authors declare no competing financial interest.

ABBREVIATIONS

OX, Orexin receptors; OX1, OX1R_HUMAN, Orexin-1 receptor; OX2, OX2R_HUMAN, Orexin-2 receptor; MD, molecular dynamics; SDM, site-directed mutagenesis; Almorexant, (2R)-2-{(1S)-6,7-Dimethoxy-1-[2-(4-trifluoromethylphenyl)ethyl]-3,4-dihydro-1H-isoquinolin-2-yl}-N-methyl-2-phenyl-acetamide; EMPA, N-ethyl-2-[(6-methoxy-pyridin-3-yl)(toluene-2-sulfonyl)amino]-N-pyridin-3-ylmethyl-acetamide; SB-674042, 1-[5-(2-fluorophenyl)-2-methylthiazol-4-yl]-1-[(S)-2-(5-phenyl-1,3,4-oxadiazol-2-ylmethyl)pyrrolidin-1-yl]methanone; GPCRs, G-protein-coupled receptors; 3D, three-dimensional; 7TMD, seven-transmembrane domain; TM, transmembrane helix; ECL, extracellular loop; β2AR, ADRB2_-HUMAN, β2-adrenergic receptor; D3, DRD3_HUMAN, human dopamine D3 receptor; A_{2A}, AA2AR_HUMAN, human A_{2A} adenosine receptor; OPSD_BOVIN, bovine rhodopsin; WT, wild type; PDB, Protein Data Bank.

REFERENCES

(1) Del Cid-Pellitero, E., and Garzon, M. (2011) Hypocretin1/OrexinA-containing axons innervate locus coeruleus neurons that project to the Rat medial prefrontal cortex. Implication in the sleep-wakefulness cycle and cortical activation. *Synapse* 65, 843−857.

(2) Azizi, H., Mirnajafi-Zadeh, J., Rohampour, K., and Semnanian, S. (2010) Antagonism of orexin type 1 receptors in the locus coeruleus attenuates signs of naloxone-precipitated morphine withdrawal in rats. *Neurosci. Lett.* 482, 255−259.

(3) Laburthe, M., Voisin, T., and El Firar, A. (2010) Orexins/hypocretins and orexin receptors in apoptosis: A mini-review. *Acta Physiol. Scand.* 198, 393−402.

(4) Mazza, M., Della, M. G., Paciello, N., Mennuni, G., Bria, P., and Mazza, S. (2005) [Orexin, sleep and appetite regulation: A review]. *Clin. Ter. (Rome)* 156, 93−96.

(5) Garcia-Borreguero, D. (2000) Article reviewed: The novel brain neuropeptide, orexin-A, modulates the sleep-wake cycle of rats. *Sleep Med.* 1, 251−252.

(6) Gatfield, J., Brisbare-Roch, C., Jenck, F., and Boss, C. (2010) Orexin receptor antagonists: A new concept in CNS disorders? *ChemMedChem* 5, 1197−1214.

(7) Panula, P., Chen, Y. C., Priyadarshini, M., Kudo, H., Semenova, S., Sundvik, M., and Sallinen, V. (2010) The comparative neuroanatomy and neurochemistry of zebrafish CNS systems of relevance to human neuropsychiatric diseases. *Neurobiol. Dis.* 40, 46−57.

(8) Nakaji, K., Ikeda, A., Oka, Y., Tomimoto, H., Shimohama, S., Kanbayashi, T., and Shibasaki, H. (2005) Hypersomnia caused by isolated angiitis of the CNS. *Intern. Med. (Tokyo, Jpn.)* 44, 883−885.

(9) Krout, K. E., Mettenleiter, T. C., Karpitskiy, V., Nguyen, X. V., and Loewy, A. D. (2005) CNS neurons with links to both mood-related cortex and sympathetic nervous system. *Brain Res.* 1050, 199−202.

(10) Burt, J., Alberto, C. O., Parsons, M. P., and Hirasawa, M. (2011) Local network regulation of orexin neurons in the lateral hypothalamus. *Am. J. Physiol.* 301, R572−R580.

(11) Gravett, N., Bhagwandin, A., Fuxe, K., and Manger, P. R. (2011) Distribution of orexin-A immunoreactive neurons and their terminal networks in the brain of the rock hyrax, *Procavia capensis*. *J. Chem. Neuroanat.* 41, 86−96.

(12) Kruger, J. L., Dell, L. A., Pettigrew, J. D., and Manger, P. R. (2010) Cellular location and major terminal networks of the orexinergic system in the brains of five microchiropteran species. *J. Chem. Neuroanat.* 40, 256−262.

(13) Nattie, E., and Li, A. (2010) Central chemoreception in wakefulness and sleep: Evidence for a distributed network and a role for orexin. *J. Appl. Physiol.* 108, 1417−1424.

(14) Malherbe, P., Roche, O., Marcuz, A., Kratzeisen, C., Wettstein, J. G., and Bissantz, C. (2010) Mapping the binding pocket of dual antagonist almorexant to human orexin 1 and orexin 2 receptors: Comparison with the selective OX1 antagonist SB-674042 and the selective OX2 antagonist N-ethyl-2-[(6-methoxy-pyridin-3-yl)-(toluene-2-sulfonyl)-amino]-N-pyridin- 3-ylmethyl-acetamide (EMPA). *Mol. Pharmacol.* 78, 81−93.

(15) Toshinai, K., Yamaguchi, H., Kageyama, H., Matsuo, T., Koshinaka, K., Sasaki, K., Shioda, S., Minamino, N., and Nakazato, M. (2010) Neuroendocrine regulatory peptide-2 regulates feeding behavior via the orexin system in the hypothalamus. *Am. J. Physiol.* 299, E394−E401.

(16) Acuna-Goycolea, C., and van den Pol, A. N. (2009) Neuroendocrine proopiomelanocortin neurons are excited by hypocretin/orexin. *J. Neurosci. 29*, 1503−1513.

(17) Gvilia, I. (2010) Underlying brain mechanisms that regulate sleep-wakefulness cycles. *Int. Rev. Neurobiol. 93*, 1−21.

(18) Makela, K. A., Wigren, H. K., Zant, J. C., Sakurai, T., Alhonen, L., Kostin, A., Porkka-Heiskanen, T., and Herzig, K. H. (2010) Characterization of sleep-wake patterns in a novel transgenic mouse line overexpressing human prepro-orexin/hypocretin. *Acta Physiol. Scand. 198*, 237−249.

(19) Appelbaum, L., Wang, G. X., Maro, G. S., Mori, R., Tovin, A., Marin, W., Yokogawa, T., Kawakami, K., Smith, S. J., Gothilf, Y., Mignot, E., and Mourrain, P. (2009) Sleep-wake regulation and hypocretin-melatonin interaction in zebrafish. *Proc. Natl. Acad. Sci. U.S.A. 106*, 21942−21947.

(20) Borgland, S. L., Taha, S. A., Sarti, F., Fields, H. L., and Bonci, A. (2006) Orexin A in the VTA is critical for the induction of synaptic plasticity and behavioral sensitization to cocaine. *Neuron 49*, 589−601.

(21) Choi, D. L., Davis, J. F., Fitzgerald, M. E., and Benoit, S. C. (2010) The role of orexin-A in food motivation, reward-based feeding behavior and food-induced neuronal activation in rats. *Neuroscience 167*, 11−20.

(22) Burgess, C. R., Tse, G., Gillis, L., and Peever, J. H. (2010) Dopaminergic regulation of sleep and cataplexy in a murine model of narcolepsy. *Sleep 33*, 1295−1304.

(23) Bubser, M., Fadel, J. R., Jackson, L. L., Meador-Woodruff, J. H., Jing, D., and Deutch, A. Y. (2005) Dopaminergic regulation of orexin neurons. *Eur. J. Neurosci. 21*, 2993−3001.

(24) Kageyama, H., Takenoya, F., Shiba, K., and Shioda, S. (2010) Neuronal circuits involving ghrelin in the hypothalamus-mediated regulation of feeding. *Neuropeptides 44*, 133−138.

(25) Fujita, W., Takahashi, M., and Tokuyama, S. (2010) [The mechanism of the development of drug dependence]. *Nihon Rinsho 68*, 1445−1450.

(26) Georgescu, D., Zachariou, V., Barrot, M., Mieda, M., Willie, J. T., Eisch, A. J., Yanagisawa, M., Nestler, E. J., and DiLeone, R. J. (2003) Involvement of the lateral hypothalamic peptide orexin in morphine dependence and withdrawal. *J. Neurosci. 23*, 3106−3111.

(27) Benoit, S. C., Clegg, D. J., Woods, S. C., and Seeley, R. J. (2005) The role of previous exposure in the appetitive and consummatory effects of orexigenic neuropeptides. *Peptides 26*, 751−757.

(28) Rodgers, R. J., Halford, J. C., Nunes de Souza, R. L., Canto de Souza, A. L., Piper, D. C., Arch, J. R., Upton, N., Porter, R. A., Johns, A., and Blundell, J. E. (2001) SB-334867, a selective orexin-1 receptor antagonist, enhances behavioural satiety and blocks the hyperphagic effect of orexin-A in rats. *Eur. J. Neurosci. 13*, 1444−1452.

(29) Sakurai, T. (2007) Regulatory mechanism of sleep/wakefulness states by orexin. *Tanpakushitsu Kakusan Koso 52*, 1840−1848.

(30) Li, Y., Li, S., Wei, C., Wang, H., Sui, N., and Kirouac, G. J. (2010) Orexins in the paraventricular nucleus of the thalamus mediate anxiety-like responses in rats. *Psychopharmacology (Berlin, Ger.) 212*, 251−265.

(31) Suzuki, M., Beuckmann, C. T., Shikata, K., Ogura, H., and Sawai, T. (2005) Orexin-A (hypocretin-1) is possibly involved in generation of anxiety-like behavior. *Brain Res. 1044*, 116−121.

(32) Johnson, P. L., Truitt, W., Fitz, S. D., Minick, P. E., Dietrich, A., Sanghani, S., Traskman-Bendz, L., Goddard, A. W., Brundin, L., and Shekhar, A. (2010) A key role for orexin in panic anxiety. *Nat. Med. 16*, 111−115.

(33) Piper, D. C., Upton, N., Smith, M. I., and Hunter, A. J. (2000) The novel brain neuropeptide, orexin-A, modulates the sleep-wake cycle of rats. *Eur. J. Neurosci. 12*, 726−730.

(34) Lee, J. H., Bang, E., Chae, K. J., Kim, J. Y., Lee, D. W., and Lee, W. (1999) Solution structure of a new hypothalamic neuropeptide, human hypocretin-2/orexin-B. *Eur. J. Biochem. 266*, 831−839.

(35) Sakurai, T., Amemiya, A., Ishii, M., Matsuzaki, I., Chemelli, R. M., Tanaka, H., Williams, S. C., Richarson, J. A., Kozlowski, G. P., Wilson, S., Arch, J. R., Buckingham, R. E., Haynes, A. C., Carr, S. A., Annan, R. S., McNulty, D. E., Liu, W. S., Terrett, J. A., Elshourbagy, N.

A., Bergsma, D. J., and Yanagisawa, M. (1998) Orexins and orexin receptors: A family of hypothalamic neuropeptides and G protein-coupled receptors that regulate feeding behavior. *Cell 92*, 1.

(36) Richey, S. M., and Krystal, A. D. (2011) Pharmacological advances in the treatment of insomnia. *Curr. Pharm. Des. 17*, 1471−1475.

(37) Hauw, J. J., Hausser-Hauw, C., De Girolami, U., Hasboun, D., and Seilhean, D. (2011) Neuropathology of sleep disorders: A review. *J. Neuropathol. Exp. Neurol. 70*, 243−252.

(38) Coleman, P. J., Cox, C. D., and Roecker, A. J. (2011) Discovery of dual orexin receptor antagonists (DORAs) for the treatment of insomnia. *Curr. Top. Med. Chem. 11*, 696−725.

(39) Arias-Carrion, O., and Stamelou, M. (2010) Targeting the orexin system: A new approach for treating insomnia. *CNS Neurol. Disord.: Drug Targets 9*, 667.

(40) Sullivan, S. S., and Guilleminault, C. (2009) Emerging drugs for insomnia: New frontiers for old and novel targets. *Expert Opin. Emerging Drugs 14*, 411−422.

(41) Neubauer, D. N. (2010) Almorexant, a dual orexin receptor antagonist for the treatment of insomnia. *Curr. Opin. Invest. Drugs 11*, 101−110.

(42) Malherbe, P., Borroni, E., Pinard, E., Wettstein, J. G., and Knoflach, F. (2009) Biochemical and electrophysiological character-ization of almorexant, a dual orexin 1 receptor (OX1)/orexin 2 receptor (OX2) antagonist: Comparison with selective OX1 and OX2 antagonists. *Mol. Pharmacol. 76*, 618−631.

(43) Scammell, T. E., and Winrow, C. J. (2011) Orexin receptors: Pharmacology and therapeutic opportunities. *Annu. Rev. Pharmacol. Toxicol. 51*, 243−266.

(44) Yanagisawa, M. (2011) Hypothalamic orexin system: From orphan GPCR to therapeutic target. *Exp. Anim. 60*, 199.

(45) Fujimoto, T., Kunitomo, J., Tomata, Y., Nishiyama, K., Nakashima, M., Hirozane, M., Yoshikubo, S., Hirai, K., and Marui, S. (2011) Discovery of potent, selective, orally active benzoxazepine-based Orexin-2 receptor antagonists. *Bioorg. Med. Chem. Lett. 21*, 6414−6416.

(46) Perrey, D. A., Gilmour, B. P., Runyon, S. P., Thomas, B. F., and Zhang, Y. (2011) Diaryl urea analogues of SB-334867 as orexin-1 receptor antagonists. *Bioorg. Med. Chem. Lett. 21*, 2980−2985.

(47) Tran, D. T., Bonaventure, P., Hack, M., Mirzadegan, T., Dvorak, C., Letavic, M., Carruthers, N., Lovenberg, T., and Sutton, S. W. (2011) Chimeric, mutant orexin receptors show key interactions between orexin receptors, peptides and antagonists. *Eur. J. Pharmacol. 667*, 120−128.

(48) Putula, J., and Kukkonen, J. P. (2011) Mapping of the binding sites for the OX(1) orexin receptor antagonist, SB-334867, using orexin/hypocretin receptor chimaeras. *Neurosci. Lett.*, 111−115, DOI: 506.

(49) Malherbe, P., Borroni, E., Gobbi, L., Knust, H., Nettekoven, M., Pinard, E., Roche, O., Rogers-Evans, M., Wettstein, J. G., and Moreau, J. L. (2009) Biochemical and behavioural characterization of EMPA, a novel high-affinity, selective antagonist for the OX(2) receptor. *Br. J. Pharmacol. 156*, 1326−1341.

(50) Langmead, C. J., Jerman, J. C., Brough, S. J., Scott, C., Porter, R. A., and Herdon, H. J. (2004) Characterisation of the binding of [^{3}H]-SB-674042, a novel nonpeptide antagonist, to the human orexin-1 receptor. *Br. J. Pharmacol. 141*, 340−346.

(51) Obiol-Pardo, C., Lopez, L., Pastor, M., and Selent, J. (2011) Progress in the structural prediction of G protein-coupled receptors: D3 receptor in complex with eticlopride. *Proteins 79*, 1695−1703.

(52) Congreve, M., Langmead, C., and Marshall, F. H. (2011) The use of GPCR structures in drug design. *Adv. Pharmacol. 62*, 1−36.

(53) Taylor, C. M., Rockweiler, N. B., Liu, C., Rikimaru, L., Tunemalm, A. K., Kisselev, O. G., and Marshall, G. R. (2010) Using ligand-based virtual screening to allosterically stabilize the activated state of a GPCR. *Chem. Biol. Drug Des. 75*, 325−332.

(54) Congreve, M., and Marshall, F. (2010) The impact of GPCR structures on pharmacology and structure-based drug design. *Br. J. Pharmacol. 159*, 986−996.

(55) Nikiforovich, G. V., Marshall, G. R., and Baranski, T. J. (2008) Modeling molecular mechanisms of binding of the anaphylatoxin C5a to the C5a receptor. *Biochemistry 47*, 3117−3130.

(56) Becker, O. M., Dhanoa, D. S., Marantz, Y., Chen, D., Shacham, S., Cheruku, S., Heifetz, A., Mohanty, P., Fichman, M., Sharadendu, A., Nudelman, R., Kauffman, M., and Noiman, S. (2006) An integrated in silico 3D model-driven discovery of a novel, potent, and selective amidosulfonamide 5-HT1A agonist (PRX-00023) for the treatment of anxiety and depression. *J. Med. Chem. 49*, 3116−3135.

(57) Shacham, S., Marantz, Y., Bar-Haim, S., Kalid, O., Warshaviak, D., Avisar, N., Inbal, B., Heifetz, A., Fichman, M., Topf, M., Naor, Z., Noiman, S., and Becker, O. M. (2004) PREDICT modeling and in-silico screening for G-protein coupled receptors. *Proteins 57*, 51−86.

(58) Becker, O. M., Marantz, Y., Shacham, S., Inbal, B., Heifetz, A., Kalid, O., Bar-Haim, S., Warshaviak, D., Fichman, M., and Noiman, S. (2004) G protein-coupled receptors: In silico drug discovery in 3D. *Proc. Natl. Acad. Sci. U.S.A. 101*, 11304−11309.

(59) Goddard, W. A., Kim, S. K., Li, Y., Trzaskowski, B., Griffith, A. R., and Abrol, R. (2010) Predicted 3D structures for adenosine receptors bound to ligands: Comparison to the crystal structure. *J. Struct. Biol. 170*, 10−20.

(60) Bray, J. K., and Goddard, W. A., III (2008) The structure of human serotonin 2c G-protein-coupled receptor bound to agonists and antagonists. *J. Mol. Graphics Modell. 27*, 66−81.

(61) Li, Y., Zhu, F., Vaidehi, N., Goddard, W. A., Sheinerman, F., Reiling, S., Morize, I., Mu, L., Harris, K., Ardati, A., and Laoui, A. (2007) Prediction of the 3D structure and dynamics of human DP G-protein coupled receptor bound to an agonist and an antagonist. *J. Am. Chem. Soc. 129*, 10720−10731.

(62) Goddard, W. A., and Abrol, R. (2007) 3-Dimensional structures of G protein-coupled receptors and binding sites of agonists and antagonists. *J. Nutr. 137*, 1528S−1538S.

(63) Vaidehi, N., Schlyer, S., Trabanino, R. J., Floriano, W. B., Abrol, R., Sharma, S., Kochanny, M., Koovakat, S., Dunning, L., Liang, M., Fox, J. M., de Mendonca, F. L., Pease, J. E., Goddard, W. A., and Horuk, R. (2006) Predictions of CCR1 chemokine receptor structure and BX 471 antagonist binding followed by experimental validation. *J. Biol. Chem. 281*, 27613−27620.

(64) Vaidehi, N., Floriano, W. B., Trabanino, R., Hall, S. E., Freddolino, P., Choi, E. J., Zamanakos, G., and Goddard, W. A., III (2002) Prediction of structure and function of G protein-coupled receptors. *Proc. Natl. Acad. Sci. U.S.A. 99*, 12622−12627.

(65) Carlsson, J., Coleman, R. G., Setola, V., Irwin, J. J., Fan, H., Schlessinger, A., Sali, A., Roth, B. L., and Shoichet, B. K. (2011) Ligand discovery from a dopamine D3 receptor homology model and crystal structure. *Nat. Chem. Biol. 7*, 769−778.

(66) Rayan, A. (2010) New vistas in GPCR 3D structure prediction. *J. Mol. Model. 16*, 183−191.

(67) Worth, C. L., Kleinau, G., and Krause, G. (2009) Comparative sequence and structural analyses of G-protein-coupled receptor crystal structures and implications for molecular models. *PLoS One 4*, e7011.

(68) Michino, M., Abola, E., Brooks, C. L., Dixon, J. S., Moult, J., and Stevens, R. C. (2009) Community-wide assessment of GPCR structure modelling and ligand docking: GPCR Dock 2008. *Nat. Rev. Drug Discovery 8*, 455−463.

(69) Fanelli, F., De Benedetti, P. G., Raimondi, F., and Seeber, M. (2009) Computational modeling of intramolecular and intermolecular communication in GPCRs. *Curr. Protein Pept. Sci. 10*, 173−185.

(70) Fanelli, F., and De Benedetti, P. G. (2005) Computational modeling approaches to structure-function analysis of G protein-coupled receptors. *Chem. Rev. 105*, 3297−3351.

(71) Katritch, V., and Abagyan, R. (2011) GPCR agonist binding revealed by modeling and crystallography. *Trends Pharmacol. Sci. 32*, 637−643.

(72) Kufareva, I., Rueda, M., Katritch, V., Stevens, R. C., and Abagyan, R. (2011) Status of GPCR modeling and docking as reflected by community-wide GPCR Dock 2010 assessment. *Structure 19*, 1108−1126.

(73) de Graaf, C., Rein, C., Piwnica, D., Giordanetto, F., and Rognan, D. (2011) Structure-based discovery of allosteric modulators of two related class b G-protein-coupled receptors. *ChemMedChem 6*, 2159−2169.

(74) Hubbard, R. E. (2011) Structure-based drug discovery and protein targets in the CNS. *Neuropharmacology 60*, 7−23.

(75) Sela, I., Golan, G., Strajbl, M., Rivenzon-Segal, D., Bar-Haim, S., Bloch, I., Inbal, B., Shitrit, A., Ben-Zeev, E., Fichman, M., Markus, Y., Marantz, Y., Senderowitz, H., and Kalid, O. (2010) G protein coupled receptors: In silico drug discovery and design. *Curr. Top. Med. Chem. 10*, 638−656.

(76) Millar, R. P., and Newton, C. L. (2010) The year in G protein-coupled receptor research. *Mol. Endocrinol. 24*, 261−274.

(77) Schneider, M., Wolf, S., Schlitter, J., and Gerwert, K. (2011) The structure of active opsin as a basis for identification of GPCR agonists by dynamic homology modelling and virtual screening assays. *FEBS Lett. 585*, 3587−3592.

(78) Sage, C., Wang, R., and Jones, G. (2011) G-protein coupled receptors virtual screening using genetic algorithm focused chemical space. *J. Chem. Inf. Model. 51*, 1754−1761.

(79) Vilar, S., Ferino, G., Phatak, S. S., Berk, B., Cavasotto, C. N., and Costanzi, S. (2011) Docking-based virtual screening for ligands of G protein-coupled receptors: Not only crystal structures but also in silico models. *J. Mol. Graphics Modell. 29*, 614−623.

(80) Jacob, L., Hoffmann, B., Stoven, V., and Vert, J. P. (2008) Virtual screening of GPCRs: An in silico chemogenomics approach. *BMC Bioinf. 9*, 363.

(81) Radestock, S., Weil, T., and Renner, S. (2008) Homology model-based virtual screening for GPCR ligands using docking and target-biased scoring. *J. Chem. Inf. Model. 48*, 1104−1117.

(82) Engel, S., Skoumbourdis, A. P., Childress, J., Neumann, S., Deschamps, J. R., Thomas, C. J., Colson, A. O., Costanzi, S., and Gershengorn, M. C. (2008) A virtual screen for diverse ligands: Discovery of selective G protein-coupled receptor antagonists. *J. Am. Chem. Soc. 130*, 5115−5123.

(83) Cavasotto, C. N., Orry, A. J., Murgolo, N. J., Czarniecki, M. F., Kocsi, S. A., Hawes, B. E., O'Neill, K. A., Hine, H., Burton, M. S., Voigt, J. H., Abagyan, R. A., Bayne, M. L., and Monsma, F. J., Jr. (2008) Discovery of novel chemotypes to a G-protein-coupled receptor through ligand-steered homology modeling and structure-based virtual screening. *J. Med. Chem. 51*, 581−588.

(84) Chen, J. Z., Wang, J., and Xie, X. Q. (2007) GPCR structure-based virtual screening approach for CB2 antagonist search. *J. Chem. Inf. Model. 47*, 1626−1637.

(85) Evers, A., and Klabunde, T. (2005) Structure-based drug discovery using GPCR homology modeling: Successful virtual screening for antagonists of the α1A adrenergic receptor. *J. Med. Chem. 48*, 1088−1097.

(86) Tautermann, C. S. (2011) The use of G-protein coupled receptor models in lead optimization. *Future Med. Chem. 3*, 709−721.

(87) Hoffert, J. D., Pisitkun, T., Saeed, F., Song, J. H., Chou, C. L., and Knepper, M. A. (2011) Dynamics of the G protein-coupled vasopressin V2 receptor signaling network revealed by quantitative phosphoproteomics. *Mol. Cell. Proteomics 11*, M111.014613.

(88) Bockenhauer, S., Furstenberg, A., Yao, X. J., Kobilka, B. K., and Moerner, W. E. (2011) Conformational dynamics of single G protein-coupled receptors in solution. *J. Phys. Chem. B 115*, 13328−13338.

(89) Rodriguez, D., Pineiro, A., and Gutierrez-de-Teran, H. (2011) Molecular dynamics simulations reveal insights into key structural elements of adenosine receptors. *Biochemistry 50*, 4194−4208.

(90) Grossfield, A. (2011) Recent progress in the study of G protein-coupled receptors with molecular dynamics computer simulations. *Biochim. Biophys. Acta 1808*, 1868−1878.

(91) Simpson, L. M., Wall, I. D., Blaney, F. E., and Reynolds, C. A. (2011) Modeling GPCR active state conformations: the β_2-adrenergic receptor. *Proteins 79*, 1441−1457.

(92) Bruno, A., Guadix, A. E., and Costantino, G. (2009) Molecular dynamics simulation of the heterodimeric mGluR2/5HT(2A)

complex. An atomistic resolution study of a potential new target in psychiatric conditions. *J. Chem. Inf. Model. 49*, 1602−1616.

(93) Jojart, B., Kiss, R., Viskolcz, B., and Keseru, G. M. (2008) Activation mechanism of the human histamine H4 receptor: An explicit membrane molecular dynamics simulation study. *J. Chem. Inf. Model. 48*, 1199−1210.

(94) Kimura, S. R., Tebben, A. J., and Langley, D. R. (2008) Expanding GPCR homology model binding sites via a balloon potential: A molecular dynamics refinement approach. *Proteins 71*, 1919−1929.

(95) Hallmen, C., and Wiese, M. (2006) Molecular dynamics simulation of the human adenosine A3 receptor: Agonist induced conformational changes of Trp243. *J. Comput.-Aided Mol. Des. 20*, 673−684.

(96) Filizola, M., Wang, S. X., and Weinstein, H. (2006) Dynamic models of G-protein coupled receptor dimers: Indications of asymmetry in the rhodopsin dimer from molecular dynamics simulations in a POPC bilayer. *J. Comput.-Aided Mol. Des. 20*, 405−416.

(97) Schlegel, B., Sippl, W., and Holtje, H. D. (2005) Molecular dynamics simulations of bovine rhodopsin: Influence of protonation states and different membrane-mimicking environments. *J. Mol. Model. 12*, 49−64.

(98) Ballesteros, J. A., and Weinstein, H. (1995) Integrated methods for construction three dimensional models and computational probing of structure-function relations in G protein-coupled receptors. *Methods Neurosci. 25*, 366−428.

(99) Chien, E. Y., Liu, W., Zhao, Q., Katritch, V., Han, G. W., Hanson, M. A., Shi, L., Newman, A. H., Javitch, J. A., Cherezov, V., and Stevens, R. C. (2010) Structure of the human dopamine D3 receptor in complex with a D2/D3 selective antagonist. *Science 330*, 1091−1095.

(100) Cherezov, V., Rosenbaum, D. M., Hanson, M. A., Rasmussen, S. G., Thian, F. S., Kobilka, T. S., Choi, H. J., Kuhn, P., Weis, W. I., Kobilka, B. K., and Stevens, R. C. (2007) High-resolution crystal structure of an engineered human β2-adrenergic G protein-coupled receptor. *Science 318*, 1258−1265.

(101) Jaakola, V. P., and Ijzerman, A. P. (2010) The crystallographic structure of the human adenosine A2A receptor in a high-affinity antagonist-bound state: Implications for GPCR drug screening and design. *Curr. Opin. Struct. Biol. 20*, 401−414.

(102) Palczewski, K., Kumasaka, T., Hori, T., Behnke, C. A., Motoshima, H., Fox, B. A., Le Trong, I., Teller, D. C., Okada, T., Stenkamp, R. E., Yamamoto, M., and Miyano, M. (2000) Crystal structure of rhodopsin: A G protein-coupled receptor. *Science 289*, 739−745.

(103) Needleman, S. B., and Wunsch, C. D. (1970) A general method applicable to the search for similarities in the amino acid sequence of two proteins. *J. Mol. Biol. 48*, 443−453.

(104) Styczynski, M. P., Jensen, K. L., Rigoutsos, I., and Stephanopoulos, G. (2008) BLOSUM62 miscalculations improve search performance. *Nat. Biotechnol. 26*, 274−275.

(105) Baldwin, J. M. (1993) The probable arrangement of the helices in G protein-coupled receptors. *EMBO J. 12*, 1693−1703.

(106) Cobanoglu, M. C., Saygin, Y., and Sezerman, U. (2011) Classification of GPCRs using family specific motifs. *IEEE/ACM Trans. Comput. Biol. Bioinf. 8*, 1495−1508.

(107) Gloriam, D. E., Foord, S. M., Blaney, F. E., and Garland, S. L. (2009) Definition of the G protein-coupled receptor transmembrane bundle binding pocket and calculation of receptor similarities for drug design. *J. Med. Chem. 52*, 4429−4442.

(108) Gao, Q. B., and Wang, Z. Z. (2006) Classification of G-protein coupled receptors at four levels. *Protein Eng., Des. Sel. 19*, 511−516.

(109) Wistrand, M., Kall, L., and Sonnhammer, E. L. (2006) A general model of G protein-coupled receptor sequences and its application to detect remote homologs. *Protein Sci. 15*, 509−521.

(110) Bettinelli, I., Graziani, D., Marconi, C., Pedretti, A., and Vistoli, G. (2011) The approach of conformational chimeras to model the role of proline-containing helices on GPCR mobility: The fertile case of Cys-LTR1. *ChemMedChem 6*, 1217−1227.

(111) Langelaan, D. N., Wieczorek, M., Blouin, C., and Rainey, J. K. (2010) Improved helix and kink characterization in membrane proteins allows evaluation of kink sequence predictors. *J. Chem. Inf. Model. 50*, 2213−2220.

(112) Hall, S. E., Roberts, K., and Vaidehi, N. (2009) Position of helical kinks in membrane protein crystal structures and the accuracy of computational prediction. *J. Mol. Graphics Modell. 27*, 944−950.

(113) Yohannan, S., Faham, S., Yang, D., Whitelegge, J. P., and Bowie, J. U. (2004) The evolution of transmembrane helix kinks and the structural diversity of G protein-coupled receptors. *Proc. Natl. Acad. Sci. U.S.A. 101*, 959−963.

(114) Fechteler, T., Dengler, U., and Schomburg, D. (1995) Prediction of protein three-dimensional structures in insertion and deletion regions: A procedure for searching data bases of representative protein fragments using geometric scoring criteria. *J. Mol. Biol. 253*, 114−131.

(115) Courcot, B., and Bridgeman, A. J. (2011) Modeling the interactions between polyoxometalates and their environment. *J. Comput. Chem. 32*, 3143−3153.

(116) van der Spoel, D., Lindahl, E., Hess, B., Groenhof, G., Mark, A. E., and Berendsen, H. J. (2005) GROMACS: Fast, flexible, and free. *J. Comput. Chem. 26*, 1701−1718.

(117) Hess, B., Kutzner, C., van Der Spoel, D., and Lindahl, E. (2008) GROMACS 4 Algorithms for Highly Efficient, Load-Balanced, and Scalable Molecular Simulation. *J. Chem. Theory Comput. 4*, 435−447.

(118) Jorgensen, W., Maxwell, L. D. S., and Tirado, R. J. (1996) Development and testing of the OPLS all-atom force field on conformational energetics and properties of organic liquids. *J. Am. Chem. Soc. 118*, 11225−11236.

(119) Kaminski, G. A., Friesner, J., Tirado, R. J., and Jorgensen, W. (2001) Evaluation and reparameterization of the OPLS-AA force field for proteins via comparison with accurate quantum chemical calculations on peptides. *J. Phys. Chem. B 105*, 6474−6487.

(120) Jorgensen, W., Chandresekhar, J. D., Madura, R. W., Impey, W. R., and Klein, M. L. (2012) Comparison of simple potential functions for simulating liquid water. *J. Chem. Phys. 79*, 935.

(121) Van-Gunsteren, W. F., and Berensden, H. J. C. (1988) A leap-frog algorithm for stochastic dynamics. *Mol. Simul. 1*, 173−185.

(122) Wolf, M. G., Hoefling, M., Aponte-Santamaria, C., Grubmuller, H., and Groenhof, G. (2010) g_membed: Efficient insertion of a membrane protein into an equilibrated lipid bilayer with minimal perturbation. *J. Comput. Chem. 31*, 2169−2174.

(123) Berensden, H. J. C., Postma, J. P. M., Van-Gunsteren, W. F., DiNola, A., and Haak, J. R. (1984) Molecular-Dynamics with Coupling to an External Bath. *J. Chem. Phys. 81*, 3684−3690.

(124) Essman, U., Perera, M. J., Berkowitz, T., and Darden, H. (1995) A smooth particle mesh Ewald method. *J. Chem. Phys. 103*, 8577−8593.

(125) Hess, B. J., Bekker, H. J. C., Berensden, H. J. C., and Fraajie, J. G. E. M. (1997) LINCS: A linear constraint solver for molecular simulations. *J. Comput. Chem. 18*, 1463−1472.

(126) Morozov, A. V., Kortemme, T., Tsemekhman, K., and Baker, D. (2004) Close agreement between the orientation dependence of hydrogen bonds observed in protein structures and quantum mechanical calculations. *Proc. Natl. Acad. Sci. U.S.A. 101*, 6946−6951.

(127) Salonen, L. M., Ellermann, M., and Diederich, F. (2011) Aromatic rings in chemical and biological recognition: Energetics and structures. *Angew. Chem., Int. Ed. 50*, 4808−4842.

(128) Verdonk, M. L., Cole, J. C., Hartshorn, M. J., Murray, C. W., and Taylor, R. D. (2003) Improved protein-ligand docking using GOLD. *Proteins 52*, 609−623.

(129) Labute, P. (2010) LowModeMD: Implicit low-mode velocity filtering applied to conformational search of macrocycles and protein loops. *J. Chem. Inf. Model. 50*, 792−800.

(130) Mohamed, M. N., Watts, H. D., Guo, J., Catchmark, J. M., and Kubicki, J. D. (2010) MP2, density functional theory, and molecular

mechanical calculations of C-H···π and hydrogen bond interactions in a cellulose-binding module-cellulose model system. *Carbohydr. Res.* 345, 1741−1751.

(131) Hascall, T., Baik, M. H., Bridgewater, B. M., Shin, J. H., Churchill, D. G., Friesner, R. A., and Parkin, G. (2002) A non-classical hydrogen bond in the molybdenum arene complex [η6-C$_6$H$_5$C$_6$H$_3$(Ph)OH]Mo(PMe$_3$)$_3$: Evidence that hydrogen bonding facilitates oxidative addition of the O-H bond. *Chem. Commun.,,* 2644−2645.

(132) Karo, J., Peterson, P., and Vendelin, M. (2012) Molecular dynamics simulations of creatine kinase and adenine nucleotide translocase in mitochondrial membrane patch. *J. Biol. Chem. 287,* 7467−7476.

(133) Isberg, V., Balle, T., Sander, T., Jorgensen, F. S., and Gloriam, D. E. (2011) G protein- and agonist-bound serotonin 5-HT2A receptor model activated by steered molecular dynamics simulations. *J. Chem. Inf. Model. 51,* 315−325.

(134) Lu, S. Y., Jiang, Y. J., Lv, J., Wu, T. X., Yu, Q. S., and Zhu, W. L. (2010) Molecular docking and molecular dynamics simulation studies of GPR40 receptor-agonist interactions. *J. Mol. Graphics Modell. 28,* 766−774.

(135) Vilardaga, J. P., Agnati, L. F., Fuxe, K., and Ciruela, F. (2010) G-protein-coupled receptor heteromer dynamics. *J. Cell Sci. 123,* 4215−4220.

(136) Yarnitzky, T., Levit, A., and Niv, M. Y. (2010) Homology modeling of G-protein-coupled receptors with X-ray structures on the rise. *Curr. Opin. Drug Discovery Dev. 13,* 317−325.

(137) Schlegel, B., Laggner, C., Meier, R., Langer, T., Schnell, D., Seifert, R., Stark, H., Holtje, H. D., and Sippl, W. (2007) Generation of a homology model of the human histamine H(3) receptor for ligand docking and pharmacophore-based screening. *J. Comput.-Aided Mol. Des. 21,* 437−453.

(138) Periole, X., Huber, T., Marrink, S. J., and Sakmar, T. P. (2007) G protein-coupled receptors self-assemble in dynamics simulations of model bilayers. *J. Am. Chem. Soc. 129,* 10126−10132.

(139) Bettica, P., Nucci, G., Pyke, C., Squassante, L., Zamuner, S., Ratti, E., Gomeni, R., and Alexander, R. (2011) Phase I studies on the safety, tolerability, pharmacokinetics and pharmacodynamics of SB-649868, a novel dual orexin receptor antagonist. *J. Psychopharmacol.,* DOI: 10.1177/0269881111408954.

(140) Renzulli, C., Nash, M., Wright, M., Thomas, S., Zamuner, S., Pellegatti, M., Bettica, P., and Boyle, G. (2011) Disposition and metabolism of [^{14}C]SB-649868, an orexin 1 and 2 receptor antagonist, in humans. *Drug Metab. Dispos. 39,* 215−227.